INVESTIGATION OF RADIATION RESISTANT POLYMER PHOTODETECTORS FOR SPACE APPLICATIONS

Edward W. Taylor

International Photonics Consultants, Inc.
30 Tierra Monte NE
Albuquerque, NM 87122

11 September 2002

FINAL REPORT

AIR FORCE RESEARCH LABORATORY
Space Vehicles Directorate
3550 Aberdeen Ave SE
AIR FORCE MATERIEL COMMAND
KIRTLAND AIR FORCE BASE, NM 87117-5776

REPORT DOCUMENTATION PAGE

Form Approved OMB No. 0704-0188

1. REPORT DATE (DD-MM-YYYY)	2. REPORT TYPE	3. DATES COVERED (FROM - TO)
11-09-2002		xx-09-2001 to xx-10-2002

4. TITLE AND SUBTITLE
INVESTIGATION OF RADIATION RESISTANT POLYMER PHOTODETECTORS FOR SPACE APPLICATIONS
Unclassified

5a. CONTRACT NUMBER
5b. GRANT NUMBER
5c. PROGRAM ELEMENT NUMBER

6. AUTHOR(S)

5d. PROJECT NUMBER
5e. TASK NUMBER
5f. WORK UNIT NUMBER

7. PERFORMING ORGANIZATION NAME AND ADDRESS
International Photonics Consultants, Inc.
30 Tierra Monte NE
Albuquerque, NM87122

8. PERFORMING ORGANIZATION REPORT NUMBER

9. SPONSORING/MONITORING AGENCY NAME AND ADDRESS
,

10. SPONSOR/MONITOR'S ACRONYM(S)
11. SPONSOR/MONITOR'S REPORT NUMBER(S)

12. DISTRIBUTION/AVAILABILITY STATEMENT
APUBLIC RELEASE
,

13. SUPPLEMENTARY NOTES

14. ABSTRACT
refer to atch

15. SUBJECT TERMS

16. SECURITY CLASSIFICATION OF:			17. LIMITATION OF ABSTRACT	18. NUMBER OF PAGES	19. NAME OF RESPONSIBLE PERSON
a. REPORT	b. ABSTRACT	c. THIS PAGE	Public Release	72	Mosher, Jan Janet.Mosher@kirtland.af.mil
Unclassified	Unclassified	Unclassified			19b. TELEPHONE NUMBER International Area Code Area Code Telephone Number DSN

AFRL-VS-TR-2002-1105

Using Government drawings, specifications, or other data included in this document for any purpose other than Government procurement does not in any way obligate the U.S. Government. The fact that the Government formulated or supplied the drawings, specifications, or other data, does not license the holder or any other person or corporation; or convey any rights or permission to manufacture, use, or sell any patented invention that may relate to them.

This report has been reviewed by the Public Affairs Office and is releasable to the National Technical Information Services (NTIS). At NTIS, it will be available to the general public, including foreign nationals.

If you change your address, wish to be removed from this mailing list, or your organization no longer employs the addressee, please notify AFRL/VSSS, 3550 Aberdeen Ave SE, Kirtland AFB, NM 87117-5776.

Do not return copies of this report unless contractual obligations or notice on a specific document requires its return.

This report has been approved for publication.

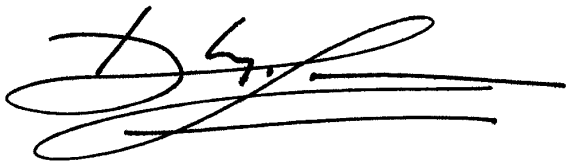

DANG T. LE, 1st LT, USAF
Project Manager

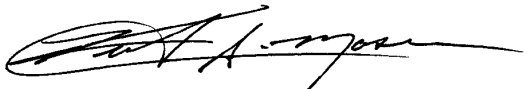

KIRT S. MOSER, DR-IV
Chief, Spacecraft Technology Division

REPORT DOCUMENTATION PAGE

Form Approved
OMB No. 0704-0188

1. REPORT DATE *(DD-MM-YYYY)*	**2. REPORT TYPE**	**3. DATES COVERED** *(From - To)*
11-09-2002	Final Report	14-09-2001 To 14-10-2002

4. TITLE AND SUBTITLE
Investigation of Radiation Resistant Polymer Photodetectors for Space Applications

5a. CONTRACT NUMBER
F29601-01-C-0261

5b. GRANT NUMBER

5c. PROGRAM ELEMENT NUMBER
62601F

6. AUTHOR(S)
Edward W. Taylor

5d. PROJECT NUMBER
4846

5e. TASK NUMBER
CR

5f. WORK UNIT NUMBER
A1

7. PERFORMING ORGANIZATION NAME(S) AND ADDRESS(ES)

International Photonics Consultants, Inc.
30 Tierra Monte NE
Albuquerque, NM 87122

8. PERFORMING ORGANIZATION REPORT NUMBER

9. SPONSORING / MONITORING AGENCY NAME(S) AND ADDRESS(ES)
Air Force Research Laboratory
Space Vehicles Directorate
3550 Aberdeen Ave., SE
Kirtland AFB, NM 87117-5776

10. SPONSOR/MONITOR'S ACRONYM(S)
AFRL/VSSE

11. SPONSOR/MONITOR'S REPORT NUMBER(S)
AFRL-VS-TR-2002-1105

12. DISTRIBUTION / AVAILABILITY STATEMENT
APPROVED FOR PUBLIC RELEASE; DISTRIBUTION UNLIMITED.

13. SUPPLEMENTARY NOTES

14. ABSTRACT

Polymeric materials will play a pivitol role in advancing next-generation ultra-miniature high bandwidth cost effective photonic, optoelectronic and electrooptic systems for space applications. Polymer photodetectors (PPDs) may play a pivitol role for rapid development of robust efficient and radiation resistant space sensor systems. Several photovoltaic detector types composed of Ruthenium Complex and of poly (p-phenylene vinylene)-sulfonated polystyrene were fabricated using electrostatic self-assembly processing. The PPDs were characterized and studied for their resistance to gamma-ray-ionizing radiation. A comparison of the pre- and post- irradiation responses of the two classes of PPDs resulted in ionization-induced changes to quantum efficiencies, response times, material conductivities, output photovoltages, short circuit currents and short circuit voltages. The data and results of the preliminary investigation strongly indicated that the use of molecular self-assembly processing can be used to develop space-radiation resistant PPDs with improved quantum efficiencies at near-IR wavelengths.

15. SUBJECT TERMS
Polymer Photodetectors, Radiation Hardening, Radiation Resistance, Radiation Effects, Space Environments, Gamma-Rays, Space Radiation Effects, Gratzel Cells, Photovoltaic Detectors, Photonics

16. SECURITY CLASSIFICATION OF:			**17. LIMITATION OF ABSTRACT**	**18. NUMBER OF PAGES**	**19a. NAME OF RESPONSIBLE PERSON**
a. REPORT	**b. ABSTRACT**	**c. THIS PAGE**			Lt Dang Le
Unclassified	Unclassified	Unclassified	Unlimited	72	**19b. TELEPHONE NUMBER** *(include area code)* (505) 846-7264

Standard Form 298 (Rev. 8-98)
Prescribed by ANSI Std. 239.18

TABLE OF CONTENTS

FIGURES

TABLES

FOREWARD

Polymeric materials will play a pivotal role in advancing next-generation ultra-miniature, high bandwidth, cost effective photonic, optoelectronic and electrooptic technology for space applications. By employing molecular engineering to achieve selective orientation of π-electrons within the polymer structure, the index of refraction and the degree of birefringence and nonlinear properties can be altered in many polymeric materials to eventually fabricate efficient and economical light emitting diodes, lasers, optical waveguides and modulators. The ability to molecularly manipulate the polarization and refractive index as well as the spectral absorption and charge transfer efficiencies in materials is important for realizing efficient and useful polymer photodetector and sensing devices. Perhaps the least evolved component of the polymer based technologies for lightwave applications is that of the optical detector, especially photodetectors that are required to operate at longer wavelengths ($\lambda > 1$ μm). However, this situation is expected to soon change as evidenced by the increased reporting of R & D results for developing organic/polymer based detectors. Organic/polymer photodetectors are expected to offer the space community many advantages compared to their inorganic counterparts, including: reduced size and weight, very low-cost, high yields, robust structures, and most importantly, flexible plastic-like arrays that have widespread potential for applications to next-generation DOD and commercial space systems. The successful application of polymeric materials to existing and next generation terrestrial, aerospace and space assets is conditional on the resistance of the materials to a myriad of environmental effects. Atmospheric, exo-atmospheric and deep space induced effects might include different combinations and varying degrees of atomic oxygen scavenging, dielectric charging, electromagnetic interference, temperature, vacuum and radiation induced degradation. Many of these adverse effects are well known for a wide variety of inorganic electronic materials and components, and to a much lesser extent for inorganic photonic components. Response data and models for understanding the physics of inter-

actions caused by ionizing radiation in photonic, optical and electronic devices based on polymeric materials grown by specific processing techniques are virtually nonexistent.

Currently, only a limited database exists from which incomplete, rudimentary theoretical models can be formulated. However, as reported in a few recent studies, several promising polymer-based electronic and photonic materials and devices have displayed significant resistance to gamma-ray and energetic (~ 64 MeV) proton irradiation, while other promising polymer photonic materials were found to be susceptible to ionizing radiation.

In order to argue effectively for developing polymer technologies for space applications, conclusive data supportive of emerging polymeric materials resistance to ionizing radiation is critical. The lack of a radiation effects data base and absence of rigorous and predictive models for assisting hardened polymer photonics device system designs, best describes the current state-of-the-art.

Unless radiation effects investigations commence early in the polymer photodetector development stages for the purpose of providing constructive feedback for influencing rapidly developing processing techniques, costly investigations for determining and implementing radiation hardening mitigation processes at later developmental stages may result.

The empirical results reported in this document provides a first but critical step in addressing these and other concerns essential for developing radiation resistant polymer photodetectors for space applications.

ACKNOWLEDGEMENTS

The "Advancement of Polymer Photodetectors for Space Applications" project was directed by Lt. Dang Le of the AFRL Space Sensing & Vehicles Control Branch (VSSS) within the AFRL Space Vehicles Directorate at Kirtland AFB, NM. Lt. Le and Dr. David Cardimona of AFRL/VSSS provided valuable technical contributions throughout the investigation which greatly contributed to the success for meeting or exceeding the goals and objectives of the research study. The fabrication of the polymer photodetectors as well as the pre-and post irradiation measurements and assistance in the interpretation of the photodetector response data were performed by: Dr. Michael Durstock of the AFRL/MLBP Polymer Branch within the AFRL Materials and Manufacturing Directorate at Wright Patterson AFB, OH; Drs. Richard Claus and Tingying Zeng of NanoSonic, Inc, Blacksburg, VA; and Mr. Barney E. Taylor of the University of Dayton Research Institute, Dayton, OH. Mr. Donald Berry of the Sandia National Laboratory Gamma-ray Irradiation Facility, Kirtland AFB, NM; and Ms. Linda R. Taylor of International Photonics Consultants (IPC), provided valuable assistance in performing the device irradiations. The teaming of two AFRL organizations with IPC and NanoSonic researchers resulted in a rapid-empirical study and assessment of state-of-the-art polymer photodetector materials and devices.

1.0 SUMMARY

1.1 Motivation

The research investigation conducted by the International Photonics Consultants, Inc., for the Air Force Research Laboratory Space Sensing & Vehicle Control Branch (VSSS) consisted of the fabrication and characterization of state-of-the-art polymer photodetectors and a preliminary evaluation of their responses to gamma-ray irradiation. Emphasis was centered on developing photodetectors fabricated by electrostatic self assembly (ESA) based processing and the tailoring of nanostucture materials. Photodetectors fabricated by the AFRL Polymer Branch (MLBP) and NanoSonic, Inc. were characterized for their pre- and post- irradiation key properties such as external quantum efficiency (EQE), photovoltage (PV), photocurrent (Isc), spectral responses and factors affecting the photo-detector stability. The objectives and goals of the investigation were met by acquiring empirical radiation response data critically required for advancing the Air Force's advocacy for supporting the development of next-generation photodetector sensing and surveillance technology based on polymer science. Investigation of the radiation resistance of polymer photodetectors at this early stage of development, will result in favorably impacting the development of a new, hardened and economically viable photodetector technology for meeting space and missile requirements.

1.2 Experiment Results

Following optical and electrical characterization of the photodetector samples, a number of the samples were irradiated by gamma-rays at the Sandia National Laboratory's Gamma-ray Irradiation Facility (GIF) located on Kirtland Air Force Base, New Mexico. Post-irradiation analyses were performed and the analysis of the empirical data revealed that all polymer photodetector samples were degraded by the ionizing radiation, but to different degrees. While the sample sets available for these studies were quite limited, certain of the data suggested a high potential for developing radiation resistant polymer photodetectors capable of operating at near-IR wavelengths. All liquid and solid polymer

photodetectors (PPDs) exhibited decreases to their output photovoltages following irradiation by gamma-rays, with the least amount of degradation observed in the solid versions. The pre-and post-irradiation response–behavior varied in identical sample sets and especially in the liquid photodetectors and are believed in part due to deterioration of the polymer materials via aging-exposure to the atmosphere (e.g. atomic oxygen and moisture) and possibly photodegradation processes. Aging can affect the stability of PPD photochemistry and photophysical stability of hole transport materials thus reducing the detector charge transport properties. The deterioration was mainly attributed to less than ideal packaging of some of the samples, allowing interaction of some samples with the ambient environment.

Since the sample size available for the irradiation study was very small, a concise and definitive interpretation of the ionization–induced effects in the solid PPDs composed of poly(p-phenylene vinylene)/sulfonated polystyrene (PPV/SPS) and Ruthenium (Ru) – Complex II (N3) based devices proved difficult, especially in scaling the output photovoltage as a function of applied dose. Both these materials indicated a potential for realizing radiation resistant PPDs based on improved designs.

Of significant interest was the apparent reduction in the output voltage for the gamma-ray irradiated Ru complex N3 devices which saturated between 51-100 krad(Si) suggesting that this material may be potentially resistant to ionizing radiation at higher doses. Resistance to ionizing radiation was also observed for a PPV/SPS PPD irradiated to a dose of 100 krad(Si). The external quantum efficiency for this PPD decreased significantly at low doses [10 and 50 krad(Si)] over the wavelength range of ~275-1150 nm but was less depressed over the visible to near IR wavelengths (630 nm < λ < 1000 nm) when irradiated to a 100 krad(Si) dose. These desireable effects observed at elevated dose suggest that trap filling may have occurred at the onset of irradiation and are a positive indication that the focused development of improved radiation resistant–long wavelength PPDs may soon prove feasible. By chemical modification of polymer materials, the absorption maximum may be shifted to shorter or longer wavelengths, thus

determining the detector spectral wavelength response and potentially providing radiation hardened devices.

2.0 INTRODUCTION

Polymer photonic devices have typically been fabricated either by spin coating, sol-gel technology or via evaporation processing. Unfortunately, due to requirements of high temperature and planar processing, these conventional manufacturing methods are not ideal for the similar fabrication of photovoltaic detector coatings on low-density polyimide substrates suitable for use in the space environment since the thickness and properties of films manufactured by these traditional methods are not uniform. One apparent difficulty in fabricating polymer semiconductor devices is that dye molecules used in the process to increase absorption of light or serve as a photosensitizer can aggregate, leading to non-efficient contact between the dye molecules and the semiconductor crystallite. The quantity of the absorbed dye is highly dependent upon the properties of the semiconductor films, such as the distribution of particle and pore size, the specific area, and morphology, as well as the physical and chemical properties.

A solution to these problems inherent in the development of efficient polymer photodetectors is to use electrostatic self-assembly (ESA) processing. ESA processing involves the coating of substrate materials by the alternate adsorption of anionic and cationic complexes of polymers, metallic nanoclusters and other molecules from water-based solutions at room temperature and pressure. By controlling the molecules deposited in each monolayer of the resulting multilayer thin film, optoelectronic and photonic devices with high efficiencies may be formed. Specifically, photon-to-electron conversion with high quantum efficiency can be achieved in layer-by-layer polymer dye-nanocrystalline semiconductor films, due to the highly effective inter-particle surface contact area at the molecular level, and, by using metal nanocluster/poly-dye multilayers to enhance optical absorbance. It is with this approach that the development of efficient polymer photodetectors for application to space systems was enjoined.

There is a general belief within the radiation effects community that photonic devices composed of polymer materials are intrinsically resistant to ionizing radiation and therefore are ideal for applications in space radiation environments. This belief has considerable merit, since many polymers are indeed primarily composed of light

elements such as H, C, N and O with low atomic numbers (AN) of 1, 6, 7, and 8, respectively. Polymers composed purely of these elements do not interact strongly with ionizing radiation (e.g. gamma-rays, x-rays, etc.) unless of course, elements of higher atomic mass are introduced into the polymeric matrix. As will be shown in this report, the development of emerging polymer photodetectors composed of exotic polymeric compounds and containing trace amounts of elements high in atomic number can and do contribute to the degradation of polymers in the presence of ionizing radiation. However, since many polymer devices are in the early stages of development, there is an excellent potential for invoking the necessary molecular engineering to mitigate unwanted radiation induced responses. Altering of the polymer chemical compositions and perfecting processing techniques early in material studies and device development to address radiation effects phenomena will provide an efficient and economic approach to realizing near-term development of polymer technologies suitable for applications in the space environment.

3.0 FABRICATION OF POLYMER PHOTODETECTORS USING ELECTROSTATIC SELF-ASSEMBLY (ESA) PROCESSING

Recent research and development in the synthesis of relatively high efficiency polymer-based optoelectronic thin film devices, including light emitting diodes (LEDs), lasers and photovoltaic (PV) devices, strongly suggests a high potential for fabricating miniature, low power PV detector arrays directly onto rigid and flexible substrate materials. The successful development of such technology could result in realizing next generation sensor technologies that can be easily stowed and deployed aboard weight and volume-constrained space systems. Recent developments in photovoltaic research based on self-assembled polymer material developments have provided the motivation for an investigation conducted by IPC, Inc. for AFRL/VSSS. The purpose and intent of the investigation was focused on determining the feasibility for eventually developing radiation resistant polymer-based photo-detectors using state-of-the-art self-assembly processing techniques.

Innovative polymer based detector research by various optoelectronic device groups, especially by Grätzel's Laboratory for Photonics and Interfaces at the Swiss Federal Institute of Technology in Lausanne, Switzerland is focused on developing high efficiency PV detectors. Grätzel has identified molecular constituents in dye-sensitized polymer-based PV devices, determined the details of the redox chemistry associated with metal nanocluster/polymer photogeneration in such devices, and, have demonstrated the processing of simple PV devices on solid substrates [1-3]. PV solar cells based on dye-sensitized mesoporous semiconductor films are low-cost alternatives to commercially available and conventional Si and GaAs solar cells [2,4]. Impressive solar-to-electrical energy conversion efficiencies have been achieved with such films when used in conjunction with liquid electrolytes [3]. Recently, Grätzel's detector group demonstrated that solid state dye sensitized solar cells may exhibit very high efficiency conversion of photons to electrical current, with remarkable yields as large as 50%, by the replacement of the liquid electrolyte with a solid charge-transport material (i.e. hole-transport material) [2].

However, the polymer materials for these devices have been fabricated either by spin coating, sol-gel technology or evaporation. Due to requirements of high temperature and planar processing, these conventional manufacturing methods are not entirely suitable for the similar fabrication of PV device coatings on low-density polyimide substrates appropriate for use in the space environment. Specifically, the Ru-based photosensitizer dye molecules in PV devices are absorbed in the porous semiconductor films by physical methods [2], and the hole-transport material is deposited by spin coating. The thickness and properties of films manufactured by these traditional methods are not uniform. One apparent difficulty is that the absorbed dye molecules aggregate, leading to non-efficient contact between the dye molecules and the semiconductor crystallite. The quantity of the absorbed dye is highly dependent upon the properties of the semiconductor films, such as the distribution of particle and pore size, the specific area, and morphology, as well as the physical and chemical properties of the materials.

3.1 ESA Processing.

A viable approach to many of the problems inherent in the development of efficient polymer photodetectors, is to use electrostatic self-assembly (ESA) processing. ESA processing involves the coating of substrate materials by the alternate adsorption of anionic and cationic complexes of polymers, metallic nanoclusters and other molecules from water-based solutions at room temperature and pressure. By controlling the molecules deposited in each monolayer of the resulting multilayer thin film, optoelectronic devices with high efficiency may be formed as shown in Figure 1.

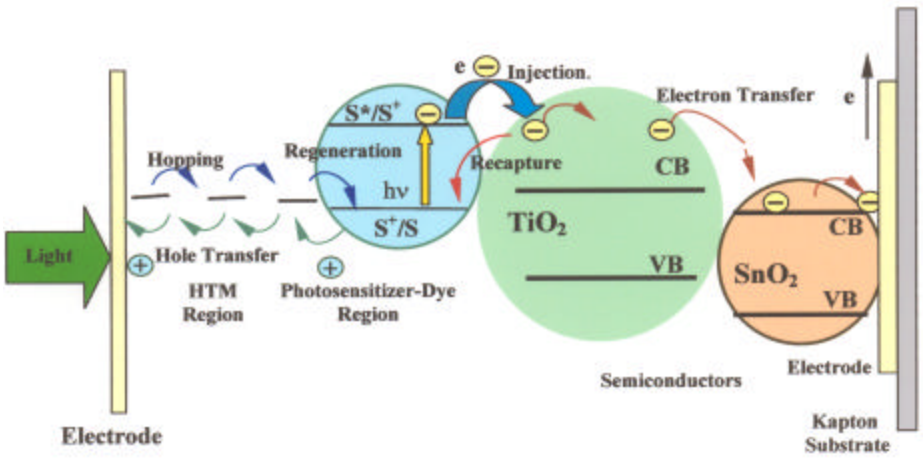

Figure 1. Electron-transfer processes occurring in a self-assembled dye-sensitized heterojunction device. Shown are the approximate relative positions of redox potentials and band energies of different components [5].

Specifically, photon-to-electron conversion with high quantum efficiency can be achieved in layer-by-layer polymer dye/nanocrystalline semiconductor films, due to the high-effective inter-particle surface contact area at the molecular level, and, by using metal nanocluster/poly-dye multilayers to enhance optical absorbance. Unlike Grätzel's multi-step synthesis process, that in addition to other processing steps requires heating of the substrate material to modify electrode resistance, ESA processing can be performed at

25 ^{o}C, thus allowing the formation of PV films on practically any substrate material. NanoSonic, Inc., (NS) a United States-based research and development organization has performed extensive work in this area, in cooperation with a large U.S. aerospace contractor and have demonstrated high quantum efficiencies in ESA-fabricated devices, and the ability to form functional thin films as coatings on mechanically flexible substrates [6-13].

3.2 Advantages of ESA Processing

ESA processing has many advantages over traditional thin-film synthesis methods for the implementation of dye-sensitized detectors on deployable substrates. ESA–grown nanostructure film leads to very high efficiency photo-induced electron transfer from excited dye molecules to semiconductor nanoparticles when illuminated by light of proper wavelength, as illustrated in Figure 1. Specifically, a semiconductor nanocrystallite can be self-assembled from ionic transition-metal poly-dye complexes into multi-layered thin films with thickness and nanostructures precisely controlled by the ESA processes through the deposited bilayer numbers, as demonstrated previously by NS team members using TiO_2 nanoclusters and dye molecules [6-9]. This approach allows excellent contact between the photosensitizer poly-dyes and the semiconductor nanocrystallites, resulting in a high injection of photoinduced electrons from dye molecules to the semiconductor nanoparticles (as shown for TiO_2 and illustrated in Figure 1). The semiconductor nanocrystallites offer quantum size effects both in bandgap and in volume as recently demonstrated by Nanosonic, Inc. researchers [5-9]. The small volume effect provides the ability for high charge transfer on its particle surface, resulting in a high efficiency collection of the photo-induced electrons on the electrodes (Figure 1). Thus, the recapture of the electrons by the positive charged dye molecules is greatly decreased and an efficient charge separation in the system is realized.

Photovoltaic (PV) cells based on wide bandgap oxides, such as TiO_2, WO_3 and ZnO nanocrystal semiconductors, sensitized by molecular dyes, have attracted recent attention in design of high performance solar cells for the conversion of sunlight to electricity and the development of photodetecting nanomachines and photovoltaic devices [14-18]. Nanocrystalline TiO_2 is of particular relevance for fabricating dye-sensitized PV cells, where photovoltaic action occurs at the junction between a porous nanocrystalline TiO_2 film and an electrolyte. During the course of this study the feasibility of using nanocrytalline TiO_2 porous films, and a synthesized Ru-complex as the photosensitizer, to design a Grätzel "liquid" cell, as shown in Figure 1 was demonstrated to have good photovoltaic behavior.

4.1 Liquid PV Cells

By fabricating liquid polymer photodetector cells, a systematic evaluation of the photogeneration performance of candidate liquid materials were investigated and evaluated as precursors to eventually fabricating solid polymer photodetectors. The design and synthesis of multiple candidate liquid precursor materials, their combination into liquid cell photodetectors, and the subsequent evaluation of the liquid material performance in test device configurations allowed quantitative evaluation of the anticipated quantum efficiency of candidate materials for advancing the development of solid detectors.

A distant goal envisioned from the successful development of liquid cells was to eventually develop methods of ink jet printing of the liquids to form "solid" versions of self-assembled photodetector devices. The liquid detector devices produced during this development stage were not intended as the final photodetector prototypes. However, they were characterized and irradiated by gamma-rays, along with the final solid detector samples in order to provide pre- and post- irradiation comparison data of the various liquid and solid detector properties (e.g.: photovoltage, spectral response, quantum efficiency, and detector material stability - also referred to as aging or reliability issues).

4.2 Design of Liquid PV Cells based on Ruthenium Complex : $Ru(ph_2Phen)_3Cl_2$

Shown in Figure 2 is a dye sensitized nanocrystalline liquid cell (i.e. based on a Grätzel cell design) that was fabricated to respond at solar spectrum wavelengths. As shown in Figure 2, P25 TiO_2 with an average particle size of 21nm, was obtained from the Degussa Company, and used to prepare mesoporous TiO_2 films. The redox mediator iodide electrolyte solution was a mixture of 0.5M potassium iodide and 0.05M iodine in water-free ethylene glycol. Tris(4,7-diphenyl-1,10-phenanthroline). Ruthenium dichloride complex $Ru(ph_2Phen)_3Cl_2$, was synthesized in-house and was chosen as the photosensitizer.

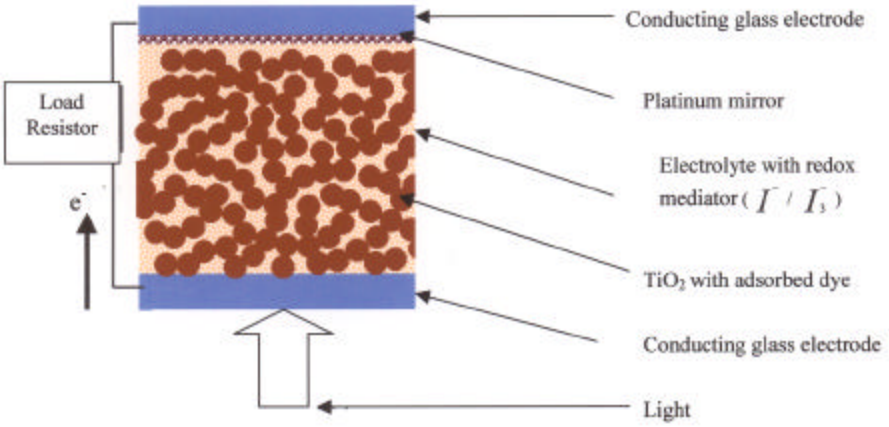

Figure 2. Diagram of a molecular dye-sensitized TiO_2 PV cell. [14,17].

In principle, the photo-excited dye transfers an electron to the semiconducting TiO_2 layer via electron injection. The injected electron is then transported through the porous TiO_2 layer and collected by an electrically conductive indium tin oxide (ITO) layer on the glass substrate surface. Within the electrolyte, the mediator (I/I_3^-) undergoes oxidation at the dye and regeneration at the counter electrode as current flows through the electrical load.

Fabrication of the cell was accomplished by first coating a TiO_2 nanocluster solution with a concentration of 0.3~0.4g/mL onto cleaned ITO-coated glass slides to form thin films

by the spin-coating method. The films were then allowed to dry in air, and further sintered in a furnace at 450 ^{0}C for 3 hours with heating rate control. The resulting TiO_2 coated conductive glass was slowly cooled down to room temperature. Next, staining of the porous TiO_2 film with ruthenium complex $Ru(ph_2Phen)_3Cl_2$ was accomplished by soaking the TiO_2-coated glass slides in a water-alcohol solution of $Ru(ph_2Phen)_3Cl_2$ (2mg/mL) for approximately 30 minutes. This resulted in a bright-yellow-stained film, that was washed first with water and then with isopropanol. Figure 3 shows the chemical structure of the $Ru(ph_2Phen)_3Cl_2$ that was synthesized by NS, and Figure 4 shows the optical absorption spectrum of this complex. As can be seen from the spectrum, the maximum absorption of this complex in the visible range is located between 430nm to 470nm.

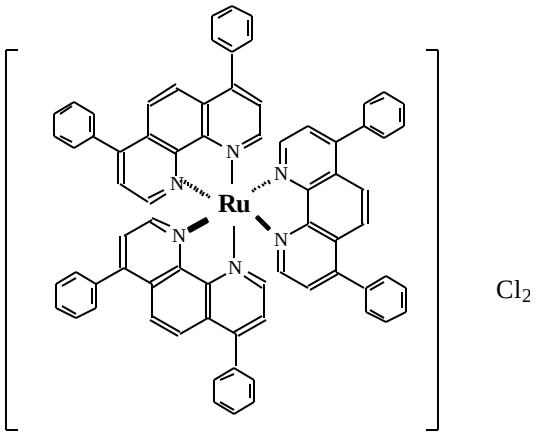

Figure 3. Chemical structure of tris(4,7-diphenyl-1,10-phenanthroline) ruthenium dichloride complex $Ru(ph_2Phen)_3Cl_2$ (denoted as N1 at Nanaosonic, Inc.).

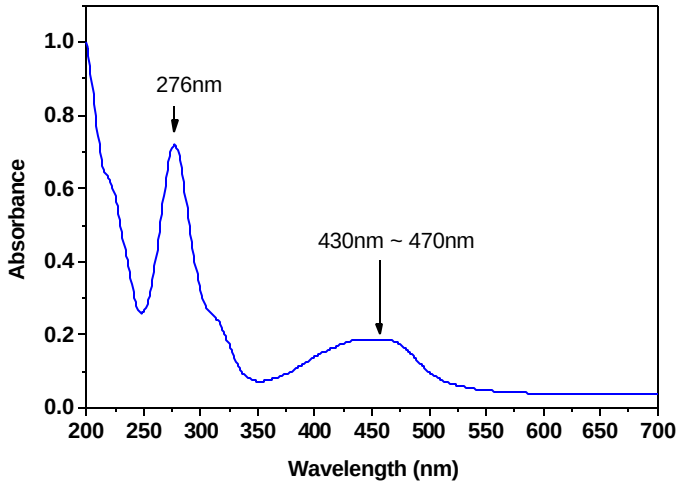

Figure 4. UV-visible optical absorption of $Ru(ph_2Phen)_3Cl_2$.

4.3 Characterization of $Ru(ph_2Phen)_3Cl_2$

Using a platinum thin film-coated electrically conductive glass slide as the counter electrode (see Figure 1), PV cells were formed by connecting the dye-stained TiO_2-coated conductive glass electrode to the counter electrode. To illuminate the dye molecules and thus to induce a photocurrent for characterization of the photo-response, a laser beam operating at a wavelength of 532nm was used as the light source. The experimental setup for the photocurrent characterization of the PV cells is schematically shown in Figure 5. Prior to performing photo-response measurements, one drop of an iodide/iodine electrolyte solution was placed at the edges of the two electrodes, and the "wet"-stained TiO_2 film to assure good contact. The photovoltaic behavior of the fabricated PV cells was then observed by monitoring the cell output voltage on an oscilloscope (shown as "OSC" in Figure 5) as the laser beam illuminated the dye-stained TiO_2 films.

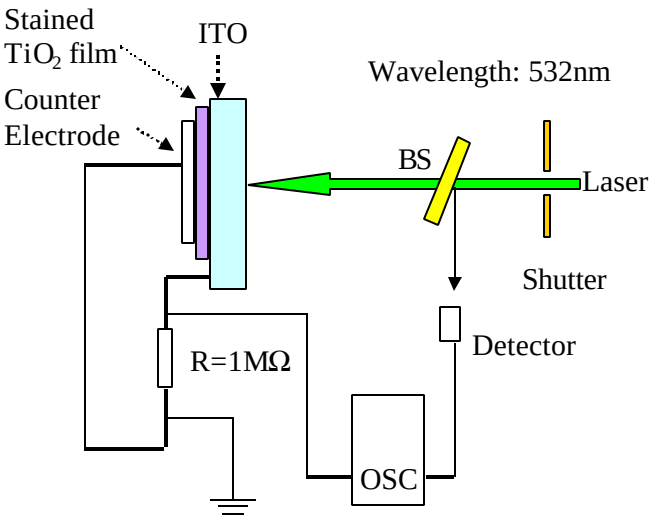

Figure 5. Setup for characterizing photovoltaic dye-sensitized PV cell behavior.

Figure 6 shows representative output voltage waveforms for the ruthenium complex stained-TiO_2 PV cells responding to laser illumination of 115.3 mW and a flash time of 5 s resulting in a maximum photovoltaic output voltage of 130 mV. As expected, the output voltage and current varied as the incident light intensity changed. The response of the cell is related to the incident light wavelength due to the electronic properties of the absorbing dye and semiconductor nanocrystals, physical construction and geometry of the device, and, the polymer material area, thickness and effective permittivity.

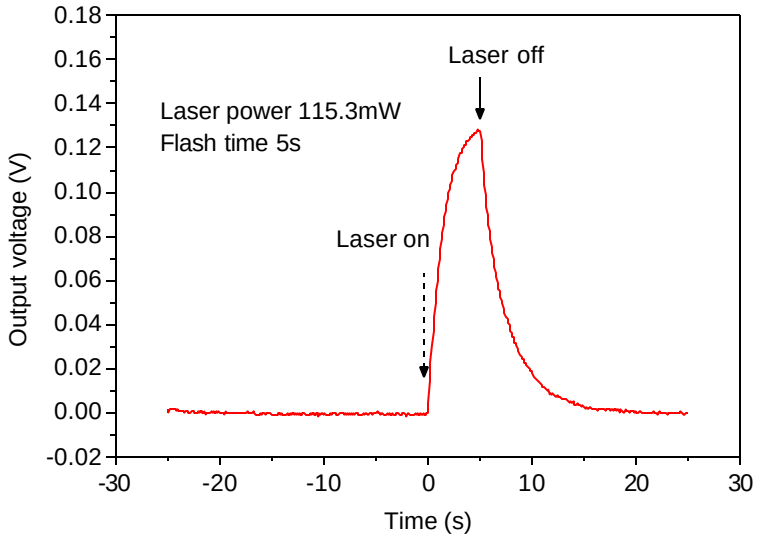

Figure 6. Photovoltaic output of ruthenium complex $Ru(ph_2Phen)_3Cl_2$ stained-TiO_2 PV cell, for a TiO_2 film thickness of 7 μm.

4.4 Improved Ru II Complex Liquid Photodetectors

Following the successful fabrication of a liquid photodetectors based on the Ru complex, improved devices were next fabricated using a new Ru-complex-sensitizer formed by NS [i.e. Cis-chloride-bis(2,2'-bypyridyl-4,4'-dicarboxylic acid) Ru II dichloride].

The chemical structure and optical absorption of the new synthesized Ru complex is shown in Figure 7. As can be seen from Figure 7, the chemical structure of this complex was designed at the molecular level by introducing carboxyl groups to improve the interaction between the photosensitizer dye molecule and the TiO_2 nanocrystalline. The modification of the Ru complex increased the efficiency of charge transfer from the excited dye molecules to the surface of the semiconductor nanocrystallines. The maximum absorption of this complex is in the visible wavelength range and located at 518 nm, which is red-shifted compared with the absorption of the Ru complex tris(4,7-diphenyl-1,10-phenanthroline) dichloride compound $Ru(ph_2Phen)_3Cl_2$ (in the region of

430 nm to 470 nm), shown in Figure 3. It should be noted that through additional modifications of this and similar polymer materials, the absorption maximum may be shifted to shorter or longer wavelengths, thus determining the detector spectral response.

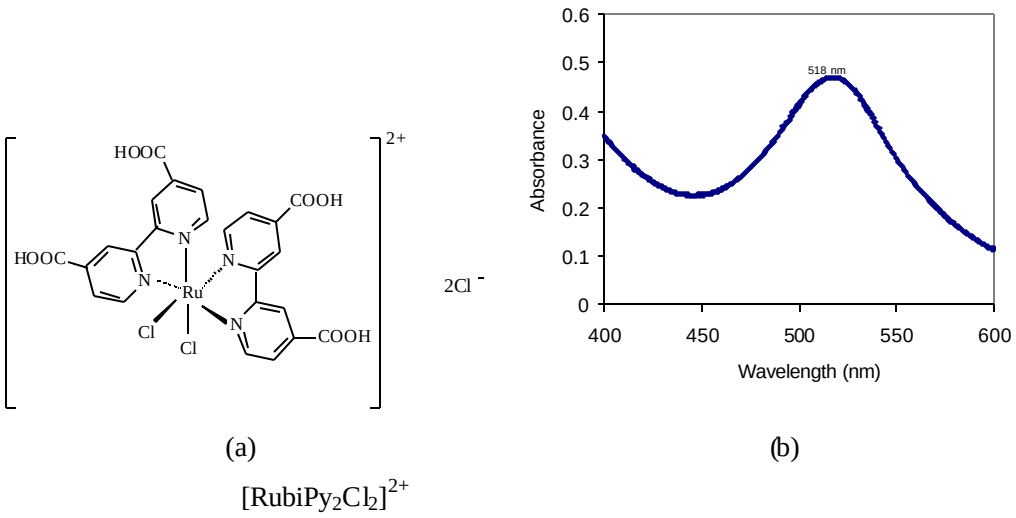

(a) (b)

$[RubiPy_2Cl_2]^{2+}$

Figure 7. Chemical structure (a) and optical absorbance (b) e of cis-chloride-bis (2,2'-bypyridyl-4,4'-dicarboxylic acid) Ru (II) dichloride complex (denoted as N2 at Nanosonic, Inc.)

The photodetector response data in Figure 7 was acquired using the laser system setup shown previously in Figure 5 to evaluate the detector response in terms of photovoltage and photocurrent. The experimental procedures used to prepare the porous TiO_2 nanocrystalline film and to stain the TiO_2 film with the improved ruthenium II complex

photosensitizer material were the same as the procedures used to fabricate the ruthenium complex liquid cell.

4.5 Packaging of Liquid Photodetectors

In order to prepare the liquid photodetectors for ease in handling and for additional pre-irradiation characterizations, the polymer material was packaged between the surfaces of two glass slides, complete with electrodes. Figure 8 is a photograph of a fabricated ruthenium complex $[RubiPy_2Cl_2]Cl_2$ stained-TiO_2 polymer photodetector (PPD). A 2 x 10^{-4} M concentration of the $Ru(ph_2Phen)_3Cl_2$ in pyridine was used to fill the space between the two electrodes, and the glass interface regions were sealed with adhesives to prevent leakage of the liquid electrolyte.

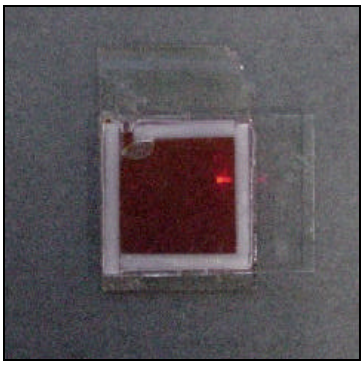

Figure 8. Packaged liquid PPD composed of $[RubiPy_2Cl_2]Cl_2$ stained-TiO_2.

The objective of this temporarily packaged cell was to allow ease in performing quantitative evaluations of the efficiency of photodetector materials as a prelude to fabricating solid versions of the liquid PPDs. The photovoltaic behavior of the packaged

PPDs were again determined using the instrumentation setup shown in Figure 5. A representative output voltage waveform responding to illumination by the laser depositing 230 mW onto the cell surface in a flash time of 1 s is shown in Figure 9. A maximum observed output photo voltage of 220 mV was measured for the improved ruthenium II complex cell. The TiO_2 film thickness for this cell was measured to be 33 µm.

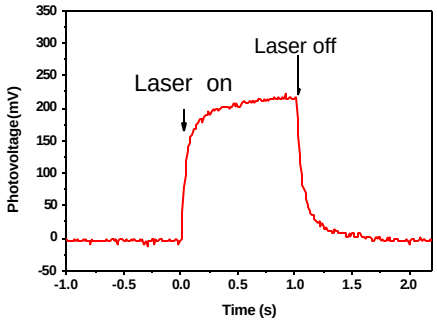

Figure 9. Ru II complex liquid photodetector response to a laser pulse. The pulse was applied for 1 s, at a wavelength of 532 nm and power of 230 mW

4.6 PPD Spectral Responses

UV-visible and near-IR response measurements were performed on the PPDs using an Oriel Model 66902 simulator as the broadband light source. To document the spectral content of this source, its output light spectrum was recorded using an Ando Optical Spectrum Analyzer (AQ-6310C), as shown in Figure 10. The output power was calibrated using an optical power meter, with and without an IR filter that blocks radiation above 800 nm. The calibration curves are shown in Figure 11.

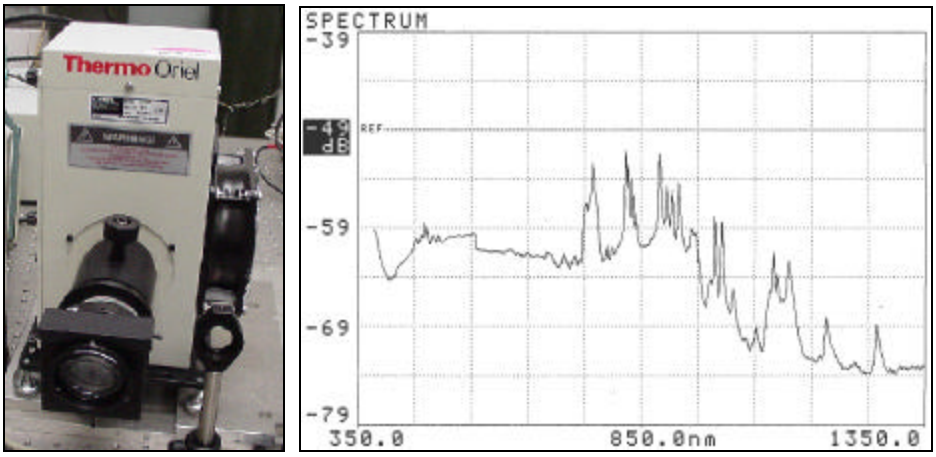

Figure 10. Broadband light source and optical spectrum

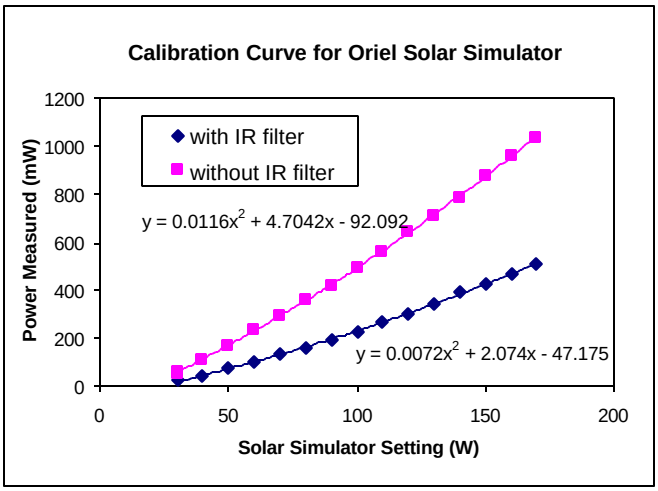

Figure 11. Broadband light source power calibration curves.

5.0 X-RAY PHOTOELECTRON SPECTROSCOPY RESULTS

To investigate the molecular photovoltaic sensitive-film interface between the TiO_2 semiconductor nanocrystal and the dye molecules, X-ray photoelectron spectroscopy (XPS) was used to analyze the dye content in the porous films. Samples were prepared by soaking sintered P_{25} TiO_2-coated ITO-glass slides in a 2×10^{-4} M solution of ruthenium

compound- (N2) - cis-chloride-bis(2,2'-bypyridyl-4,4'-dicarboxylic acid) ruthenium (II) dichloride $[RubiPy_2Cl_2]Cl_2$ (Figure 12) for 6 hours, followed by drying the samples in vacuum at room temperature. Figure 12 shows the N2 chemical structure with re-highlighted numbers (1-4) illustrating the formation of four differing covalent carbon bonds in the Ru complex. The analysis was performed using a Perkin-Elmer PHI 5400 spectrometer with a Mg Kα (1253.6 eV) achromatic X-ray source operated at 14 KV and 300 watts. The vacuum pressure inside the analysis chamber was maintained at 1×10^{-8} Torr during the analysis. The 1×1 cm film samples were mounted on a sample holder with double-sided adhesive tape. An XPS analysis of each sample was obtained over an area of 2×4 mm^2. The C1s band located at 285eV was used as a reference point for comparing the sample responses.

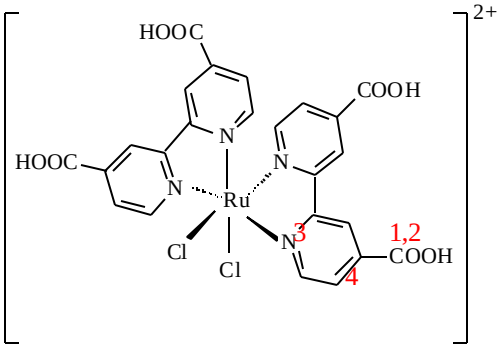

$[RubiPy_2Cl_2]^{2+}$

Figure 12. Chemical structure of N2 [cis-chloride-bis (2,2'-bypyridyl-4,4'-dicarboxylic acid) Ru (II) dichloride complex]. The red highlighted numbers (1,2,3 and 4) illustrate the formation of four differing covalent carbon bonds in the ruthenium complex.

Figure 13 represents the scan results of the film surface. As revealed by the spectroscopy results, TiO_2 is covered by an ultra thin dye molecule layer because of the strong titanium bands observed on the surface scan. Only very weak bands in the vicinity of 280eV are evident.

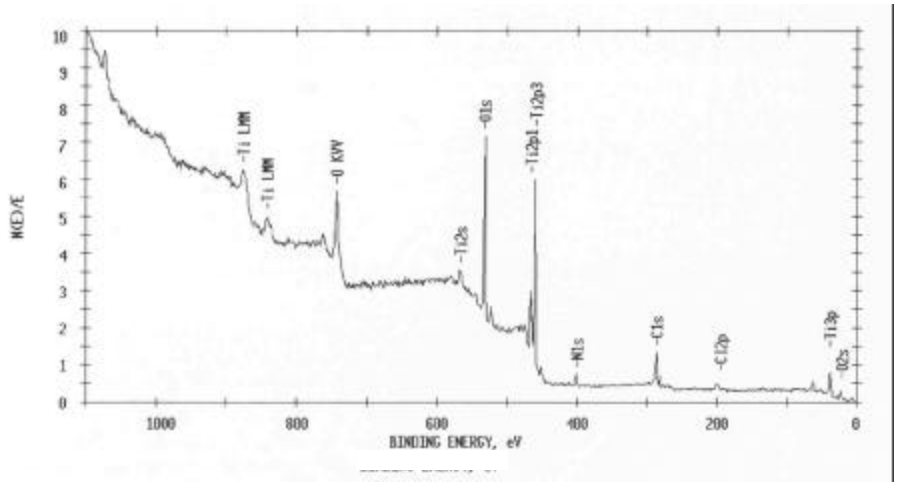

Figure 13. X-ray photoelectron spectroscopy of TiO_2-Ru complex film.

An enlarged observation of the band structure centered at 285 eV is shown in Figure 14, while shown in Figure 15 are simulated assignments (numbered 1-4) representing the elements in the binding energy regions in proximity to 284eV.

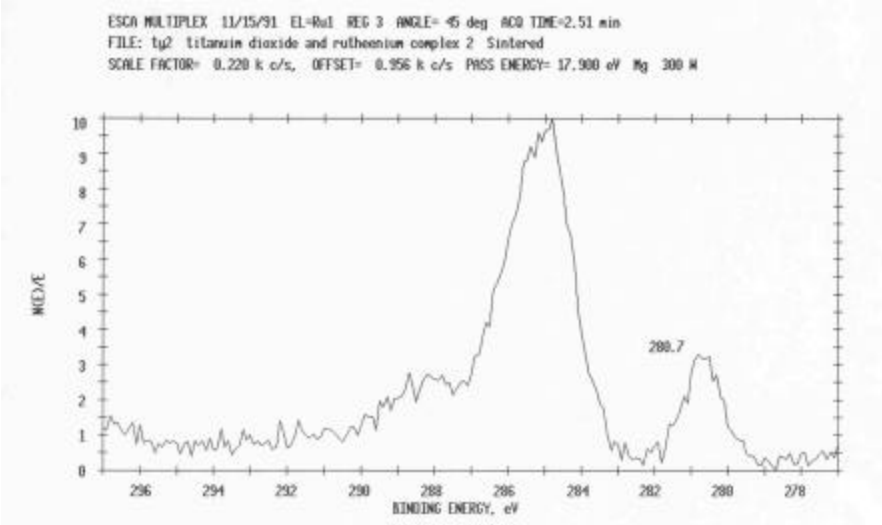

Figure 14. XPS spectrum of Ru (II) and Carbon 1s

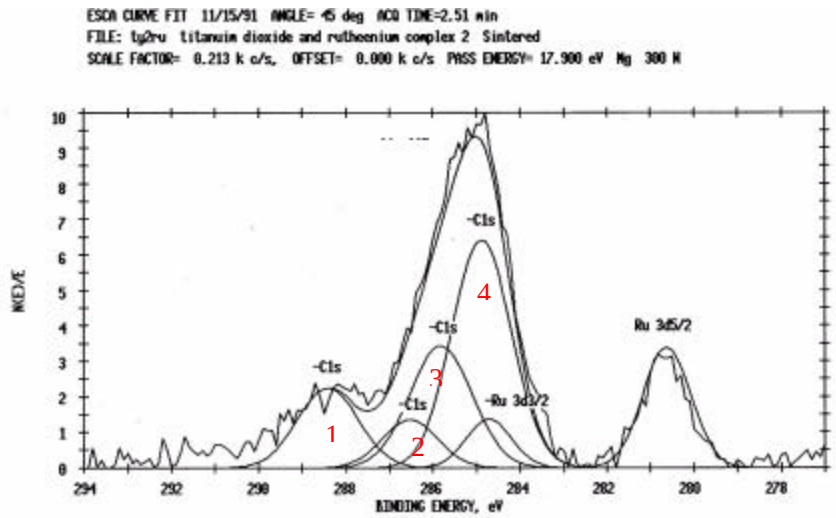

Figure 15. Simulation assignments of the XPS spectra for Ru (II) and Carbon 1s in the region around 284eV.

As can be seen from Figure 14 and Figure 15, Ru (II) $3d_{5/2}$ is present at 280.9 eV and another band of Ru (II) $3d_{3/2}$ at 284.1 eV is overlapped by the band of C1s. In addition, there are four kinds of carbon bonds existing as different covalence states in the ruthenium complex. From the higher binding energy located at around 288.5 eV to the lower binding energy at 284 eV, the C1s spectroscopy reveals C=O, C-O, C-N< and C=C chemical bonds which are indicated in the chemical structure as shown in Figures 12 and 15 as 1, 2, 3 and 4, respectively. The atomic concentration calculation using a multiplex analysis is presented in Table A-1(see Appendix A). From this analysis, it is suggested that only 0.31 at. % Ru (II) exists on the surface of the photovoltaic sensitive film.

An investigation of the interface connection between the TiO_2 nanocrystalline and the dye molecules was conducted by argon sputtering of the film to different depths. This allowed XPS analysis of the porous TiO_2/dye film within the porous film. Identification of the XPS at the film depth from surface towards the bottom of substrate at 5 nm and 10 nm yielded the same components for the survey scan results as given in Figure 13. Tables A-1, A-2, A-3 and A-4 (see Appendix A) provide the multiplex scan results for the element contents. As shown in these Tables, the concentration Ru (II) is nearly identical at 0.19 at.% for material depths of 5 nm, 10 nm and 40 nm, suggesting that the dye is

present at approximately the same concentration in the porous TiO_2 film throughout the probed volume. This implies that the dye molecules enter the pores during the staining process resulting in a uniform molecular level absorption over the TiO_2 nanocrystal surface. Therefore, the designed TiO_2/ruthenium complex sensitive film can be argued to be a molecular level-photovoltaic film.

Figure 16 illustrates the PV response of the molecular photovoltaic TiO_2-dye film PPDs. The measurement was performed using a laser operating at 230 mW at a wavelength of 532 nm and a flash time of 1 s. The PPD TiO_2 film thickness was 33 µm.

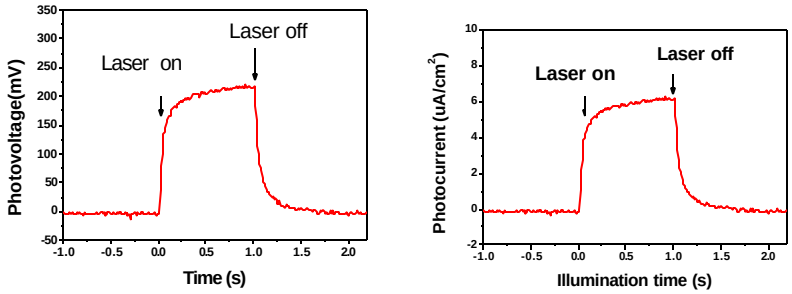

Figure 16. Laser induced photovoltage and photocurrent from Ru stained-TiO_2 films.

6.0 FABRICATION OF SOLID-ALPHA VERSION RU COMPLEX PPDS

Following the successful fabrication of liquid PPDs, solid photodetectors were next fabricated by replacing the liquid electrolyte in the liquid PPDs with solid organic hole-transport-materials (HTMs). One such HTM used to obtain improved PV performance was spiro-OMeTAD shown in Figure 17. Spiro-OMeTAD has an amorphous phase structure and a high glass transition temperature (Tg ~ 120 °C) which contribute to the desired high-efficient photon-induced hole transfer process. The spiro-OMeTAD used to fabricate the solid-α-PPDs was synthesized by American Dye Source, Inc.

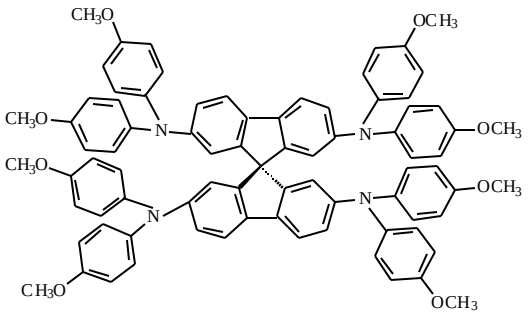

Figure 17. Chemical structure of spiro-MeOTAD.

(Canada) was prepared by dissolving 0.4 gram into 2 mL of chlorobenzene to yield a 0.17 M HTM solution. Unfortunately, the spiro HTM failed to dissolve in chlorobenzene, the most optimum solvent to be used for this compound and it was suspected that the compound was not pure. A 15 mM of N-lithiotrifluoromethane sulfonimide ($Li[(CF_3SO_2)_2N]$) was added to the HTM solution to provide a source of Li^+ ions and provided a positive charge on the surface of the TiO_2 which produced an electrostatic field, thus aiding electron injection from the dye into the semiconductor material. The next step involved forming the HTM layer which was spin-coated directly onto the P25 TiO_2 film, and followed by solvent evaporation. Copper adhesive tape was used as the counter electrode. Figure 18 displays an illustration of the cross-section of the α-version solid PPD.

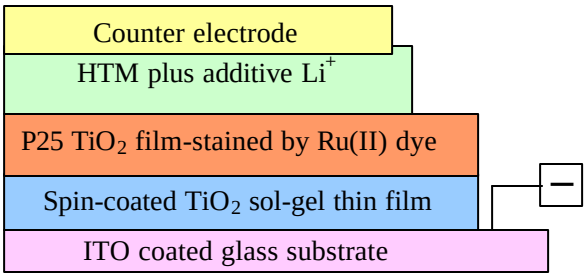

Figure 18: Cross-section of the α-version solid PPD.

Typical responses in terms of PPD output photovoltage and photocurrent are shown in Figure 20 for a 2 s illumination by a laser operating at 532 nm and 314 mW output power. As can be seen, a peak photovoltage of 2 mV in Figure 19 (a) and the corresponding peak photocurrent of 5.5 x 10^{-3} nA/cm^3 (shown in Figure 19 (b)) was achieved. This demonstrated that proper choices of a HTM and additive could improve the charge separation efficiency and allow the fabrication of solid PPDs. The TiO_2 film thickness for this PPD was 9 μm.

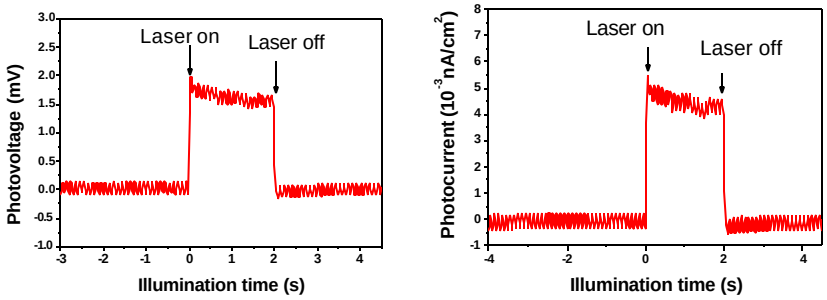

(a) (b)

Figure 19. Photovoltaic (a) and photocurrent (b) responses of an α– version PPD composed of spiro-OMeTAD as the HTM and $[RubiPy_2Cl_2]Cl_2$ as the photosensitizer.

7.0 FABRICATION OF SOLID-BETA VERSION PPDS

Improved β-versions of solid PPDs were fabricated leveraging from the processing techniques used in fabricating the α-PPDs. Substantially larger photovoltaic responses were observed in the β-PPDs. During this phase of the study, it was also demonstrated that low temperature synthesis of TiO_2 photocurrent generating film layers was possible, an important result for the potential low-cost manufacturing of PPDs in a variety of

configurations and on different substrates. The β-PPDs were fabricated using high purity spiro-OMeTAD, and modifying the HTM layer with a small amount of oxidant dopant and lithium compound, as well as by using a novel ruthenium complex sensitizer (N3), synthesized by molecular engineering techniques.

To achieve increased photogeneration response, Ru complex- cis-thiocyano-bis(2, 2'-bipyridyl-4,4'-dicarboxylate) Ru (II) complex, abbreviated ($RubiPy_2SCN_2$) and shown in Figure 20, was synthesized and termed by Nanosonic, Inc. as Ru complex 3, or N3.

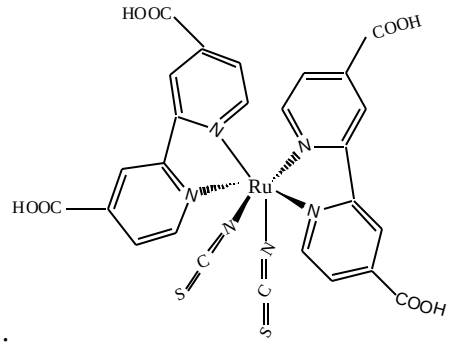

Figure 20. Chemical structure of Ruthenium complex N3.

The optical absorption curve for an aqueous solution of the Ruthenium Complex N3 is shown in Figure 21 indicating maximum absorption in the visible range near 502 nm.

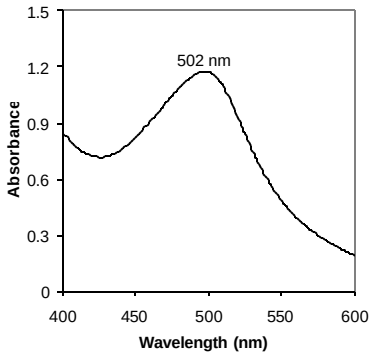

Figure 21. Optical absorption of Ruthenium complex N3 in aqueous solution.

Preparation of the PPDs required the synthesis of TiO_2 sol using sol-gel technology. A mixture of titanium alkoxide and isopropanol was slowly dripped into a mixture of glacial acetic acid and water at 0 °C under stirring, yielding a transparent sol. After hydrolyzing the titanium alkoxide in the mixture for a few hours at 80 °C, transparent nanoclusters of TiO_2 sol having a light blue color were produced.

Good quality films were formed by coating this sol onto ITO-coated glass substrates. Visually, these films appeared to be of much higher quality than films prepared using P25 TiO_2 nanocrystallines. To avoid the short-circuit problem previously experienced with the α -solid PPDs , a TiO_2 electrode film was prepared by using a sol-gel TiO_2 film as first layer and a P25 TiO_2 film as the second layer on the ITO-coated glass substrate. The film was sintered at 450 °C for 3 hours. X-ray diffraction analysis revealed that the sol-gel TiO_2 films contained anatase-type nanocrystals. Next, the TiO_2 film was stained with the Ru complex N3 by immersing the film in an N3/alcohol solution with a concentration of 1mg/mL (or 1.8×10^{-3} M of molar concentration) for 10 hours. The stained-TiO_2 electrode film was dried in a vacuum oven at room temperature for 3 hours before prior to applying the hole-transport material.

Spiro-OMeTAD obtained from COVION Organic Semiconductors (GmbH) with a purity of 99.9% was used as the HTM. A 0.17 M HTM solution was prepared by stirring the compound in chlorobenzene overnight at room temperature. The solution also contained 0.33mM of tris(4-bromophenylaminium hexachloroantimonate $N(PhBr)_3SbCl_6$ and 0.15 mM N-lithiotrifluoromethane sulfonimide ($Li[(CF_3SO_2)_2N]$). $N(PhBr)_3SbCl_6$ acts as a dopant, introducing free charge carriers in the HTM by partial oxidation of the OMeTAD. $Li[(CF_3SO_2)_2N]$ provides a positive charge on the surface of the TiO_2 and produces an electrostatic field, thus aiding electron injection from the excited-dye molecule to the conduction band of the TiO_2 semiconductor. Addition of the $N(PhBr)_3SbCl_6$ also resulted in a color change of the solution from transparent and

colorless to dark-purple. The HTM film was next coated onto the dye-stained TiO_2 film again using the spin coating process.

A counter-electrode gold film was applied to the HTM layer using a vacuum deposition method after drying the HTM layer (in a hood) at room temperature. Figure 22 illustrates the sandwich-structure of the solid polymer photodetector. The hole and electron directions within the solid-β PPD structure are also illustrated.

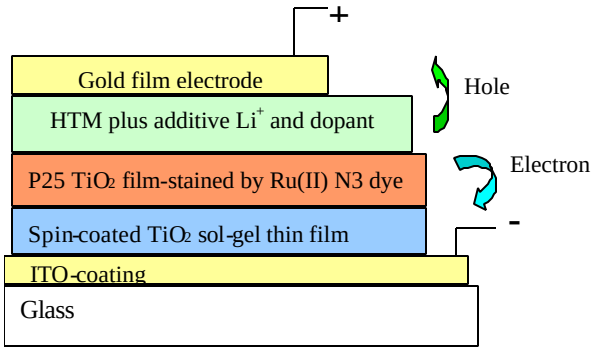

Figure 22. Schematic diagram of a solid PPD.

8.0 PPD CHARACTERIZATIONS

PPD photocurrent and output voltage response characterizations were carried out using the instrumentation arrangement shown in Figure 23. The photovoltaic response is displayed on the oscilloscope in terms of the output voltage under illumination by the solar simulator. The sample provided a maximum output voltage of 288.1 mV under

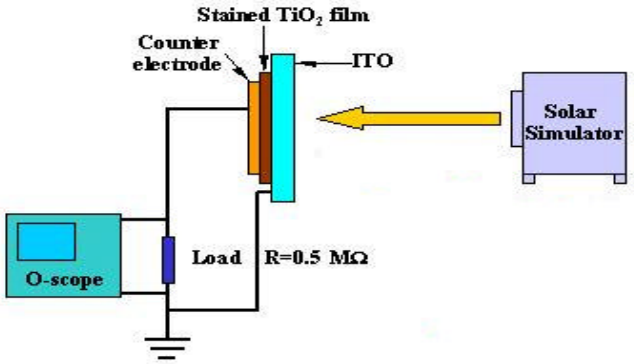

Figure 23. Instrumentation arrangement for characterizing solid PPDs.

illumination of 1.13W (using an IR filter). The PPD was illuminated from the ITO side. Shown in Figure 24 is the solar simulator-induced output voltage for a solid PPD composed of sol gel processed TiO +P25- TiO2 / Ru complex –3/Spiro-OMeTAD. The PPD was illuminated for 10 s at a simulator power of 1.13 W.

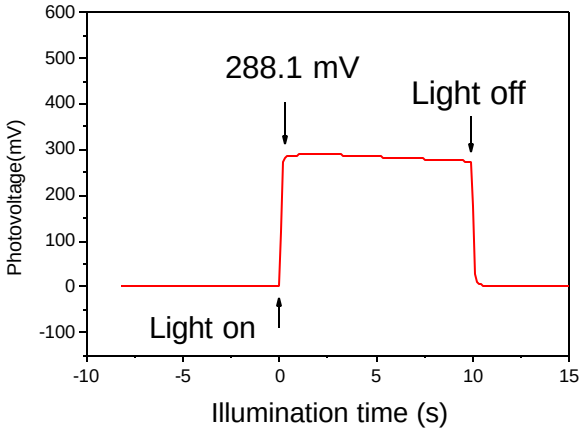

Figure 24. PV response of a sol-gel -processed TiO_2 (β)-PPD.

9.0 RADIATION EFFECTS

The successful application of polymeric materials to existing and next generation terrestrial, aerospace and space assets is pivotal on the resistance of the materials to a myriad of environmental effects. Atmospheric, exo-atmospheric and deep space induced effects might include different combinations and varying degrees of atomic oxygen scavenging, dielectric charging, electromagnetic interference, temperature, vacuum and radiation induced degradation. Many of these adverse effects are well known for a wide variety of inorganic electronic materials and components, and to a much lesser extent for inorganic photonic components [19-45]. Response data and models for understanding the physics of interactions caused in photonic, optical and electronic devices based on polymeric materials and specific processing techniques are virtually nonexistent. Currently, only a limited database exists from which incomplete, rudimentary theoretical models can be formulated [30-32,36,37,46]. It is only recently that a few publications have reported limited data or attempted to explain the effects of ionizing radiation on polymers, and even in these cases, the data focuses on radiation induced effects in polymer modulators or modulator materials.[30-32,34,36,38,46]. However, as reported in these recent studies, several promising polymer-based electronic and photonic (PBP) materials and devices have displayed significant resistance to gamma-ray and energetic (~ 64 MeV) proton irradiation.

By conducting radiation effects investigations early in PPD development stages, an understanding of the interaction of the light-matter-ionization process is possible for impacting the selection of improved radiation resistant materials. An early aggressive approach mitigates costly radiation effects-space environment investigations too often performed at a later date on highly developed, widely applied, but not necessarily radiation resistant technologies. Often during space qualification parts-testing, heroic efforts to redesign technology or to invoke costly protective measures are required for hardening new technologies “soft” to space radiation environments. The preliminary investigation of radiation resistance of polymer PPDs presented in this report are a first step to rectify this existing and all too-frequently repeated historical problem by identifying and gaining an early understanding of the effects of ionizing radiation on

emerging polymer materials and devices. While radiation induced effects are well known for variety of inorganic electronic materials and components, little is known of radiation-induced effects in emerging polymer materials and PBP devices. There is a general belief within the radiation effects community that photonic devices composed of polymer materials are intrinsically resistant to ionizing radiation and therefore are ideal for applications in space radiation environments. This belief has considerable merit, since many polymers of interest are indeed primarily composed of light elements such as H, C, N and O with low atomic numbers (AN) of 1, 6, 7, and 8, respectively. Polymers composed purely of these elements do not normally interact strongly with ionizing radiation (e.g. gamma-rays, x-rays, etc.) unless of course, elements of higher atomic mass are introduced into the polymeric matrix. As will be shown in the sections that follow, the development of emerging polymer photodetectors composed of exotic polymeric compounds and containing trace amounts of elements of moderate to high atomic number can and do contribute to PPD degradation in the presence of ionizing radiation.

9.1 Radiation Induced Effects in Self-Assembled PPDs

Recent radiation-effects data has been reported for several promising PBP materials and devices which suggest that polymer devices may soon surpass a variety of inorganic-based photonic devices in performance parameters and in resistance to gamma-ray and energetic particles (e.g. proton) [47-53]. The empirical data reported within this section is based on PPD devices fabricated via variations of ESA processing. The investigation of the effects of ionizing radiation (total dose) on three different types of PPD samples was accomplished using the Sandia National Laboratory (SNL) Gamma- Ray Irradiation Facility (GIF). Table 1 lists the PPD samples, PPD fabricator, polymer

Table 1. Listing of PPDs irradiated by gamma-rays

composition and the received gamma-ray total dose. Samples were irradiated

	Approximate Gamma-Ray Dose in krad(Si)			
NanoSonic Solid PPDs (all N3)	10	51	100	Control Samples (no irradiation)
1			x	
1A		x		
2	x			
2A				x
NanoSonic Liquid PPDs				
LD1 (N3)			x	
2 (N2)		x		
1 (N3)	x			
AFRL/MLBP Solid PPDs *(all PPV/SPS)*				
020601 A			x	
020601 B		x		
020601 C	x			

simultaneously under identical dose rate [2.01 rad(Si)/sec, +/- 3.8 %], dose and room temperature (65.8 +/- 3.45 deg. F) conditions. The samples were characterized for their pre- and post-irradiation electrical and optical responses at their points of origin (at NanoSonic, Inc. and AFRL/MLBP laboratories). Shown in Figure 25 is the arrangement

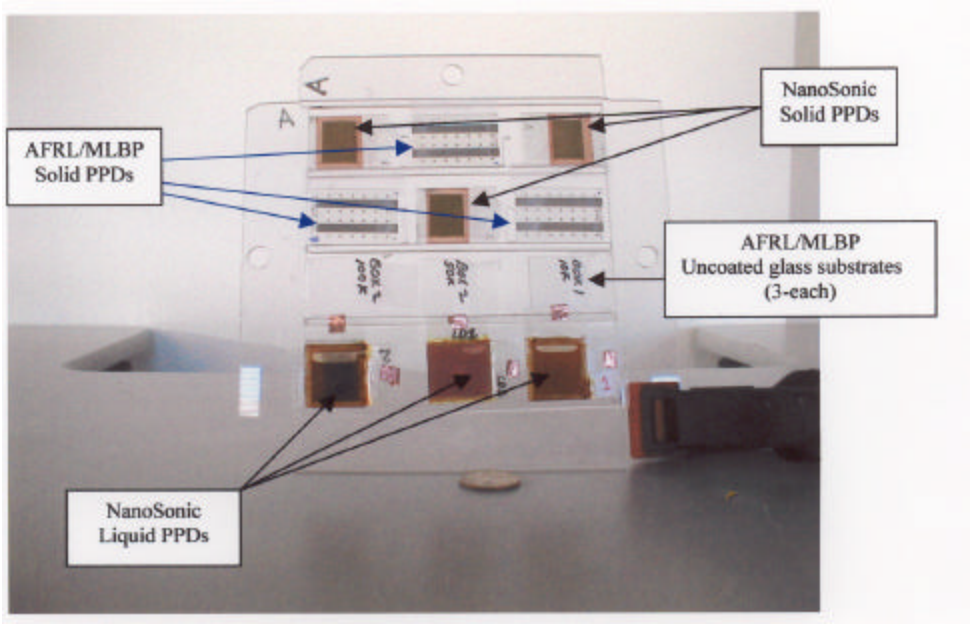

Figure 25. PPD and ancillary samples mounted on an adapter plate shown prior to irradiation by Gamma-rays.

of the NanoSonic and AFRL/MLBP PPDs, and other ancillary components mounted on an adapter plate. The adapter plate along with the samples to be irradiated were inserted within an aluminum and lead (Pb-Al) shielded container and oriented perpendicular to the gamma-ray source as shown in Figure 26. As shown in Figure 25 the samples were isolated and firmly mounted onto an 1/8 inch thick clear acrylic adaptor plate using clear adhesive tape along the sample edges. The positioning of each sample relative to its nearest neighbor was minimized in order to insure that the overall gamma-ray target area

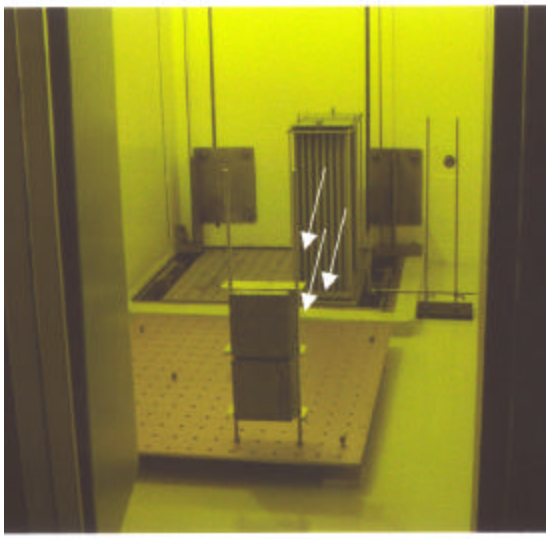

Figure 26. SNL-GIF irradiation of polymer photodetectors.

was also minimized to avoid non-uniformity in the received dose. Prior to the onset of irradiation, gamma-ray dose/dose rate mapping was accomplished to ascertain dose rate variations and to identify the spatial coordinates required for locating the samples orthogonal to the gamma-ray source. Following each of three incremental irradiations, selected samples were removed from the acrylic plate and placed in a protective storage container occupied by the control sample. Shown in Figure 26 are two stacked Pb-Al containers in which the polymer samples could be located (only the top container was used). The light colored arrows represent the direction of a portion of the emissions from the gamma-ray source in the direction of the samples.

The dosimetry considerations consisted of selecting the proper number and type of dosimeters for confidently measuring the irradiation dose, and locating the dosimeters in proximity to the samples. CaF_2 thermolumenescent detector (TLD) arrays consisting of 4 TLDs per array monitored the dose received by each sample. The array arrangement insured an accurate measurement of the gamma-ray dose received by each sample and provided multiple dose point readings for averaging the total dose across the target area.

The irradiated TLD arrays were removed following each incremental irradiation and replaced by fresh TLDs in readiness for the next incremental irradiation. The glow-curve readings of the TLDs, the dose and dose rate statistics were performed by the SNL Radiation Metrology Laboratory. The standard deviations in dose shown in Table 2 are SNL estimates based on random uncertainties in TLD responses at Co-60 energies and are reported at the 1-sigma level. At Co-60 energies, the Dose (Si) is calculated as Dose (Si) = Dose (CaF_2) x 1.02. Conversion to the SI unit of radiation absorbed dose is the Gray (Gy) where 1 Gy = 100 rad.

TABLE 2. Incremental Gamma-ray Dose and Temperature Ranges

Irradiation	**ExposureTime (minutes)**	**Dose/ Std. Dev. rad(Si)**	**Dose rate rad(Si)/sec**	**Temp.Range (deg. F)**
1	83.45	10,183 / 2.3 %	2.03	62.4-63.1
2	333.15	40,973 / 2.6 %	2.05	64.5-69.3
3	416.80	48,797 / 6.5 %	1.95	69.3-60.3

Total Dose (Run 1) = 10,183 rad(Si)

Total Dose (Run 1 + 2) = 51,156 rad(Si)

Total Dose: (1+2+3) = 99,650 rad(Si)

STD. DEV. ~ 3.80 %

Average Dose Rate = 2.01 rad(Si)/sec

9.2 PPD Pre- and Post- Irradiation Reponses

Liquid PPD 2 was composed of the Ru complex N2 and failed to operate during the post-irradiation characterizations perhaps suggesting that severe damage was induced by the 50 krad(Si) gamma-ray irradiation dose. It is also possible that the failure of the PPDs was due to degradation resulting from leakage of air and moisture into the cell volume, or due to a combination of leakage and the irradiation. The latter combination seems most

probable since leakage of the liquid polymer material from the cell was noted during the unpacking of the sample following shipment of the cell from NS to IPC. This may have rendered the deteriorated polymer sample more susceptible to experiencing additional degradation induced by the ionizing radiation. Pre- and post-irradiation measurements of the remaining liquid PPD photovoltages are shown in Figures 27 and 28, respectively.

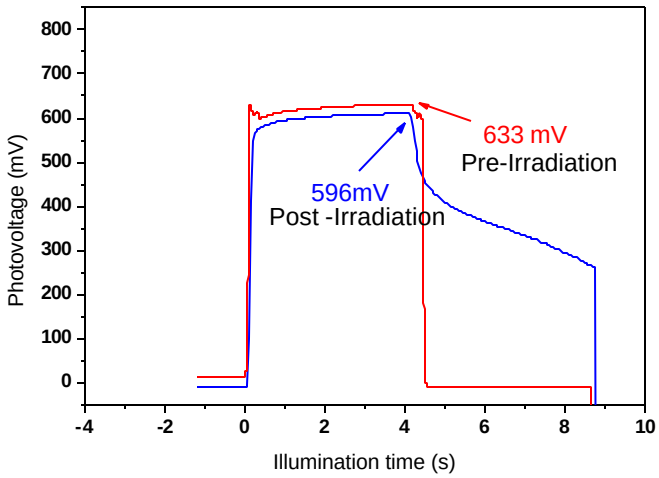

Figure 27. Post- irradiation PV response of liquid PPD 1.

In Figure 27, the post-irradiation response of liquid PPD 1 following a 10 krad (Si) dose is shown. The PPD 1 sample was composed of ruthenium complex N3 combined with iodine and iodide liquid electrolyte. The irradiated sample exhibited ~ 37 mV (6 %) reduction in its post-irradiation photovoltage output, measured one month after the gamma-ray irradiation. Quite evident in Figure 27 is the persistence of the photovoltage signal beyond the 4 s illumination period. The presence of a sustained photovoltage beyond the illumination period suggests that the conductivity of the polymer sample may have been altered due to the gamma-ray irradiation contributing to charge (carrier) trapping. The prolonged relaxation time shown in Figure 27 has also been reported for polymer gel detectors (Safarine-T dye dispersed in polyvinyl alcohol and polyethylene oxide carbonate) [54]. Relaxation times on the order of minutes in light detectors were

reported by Dey and colleagues and attributed to the slow diffusion of ions and charge trapping [54].

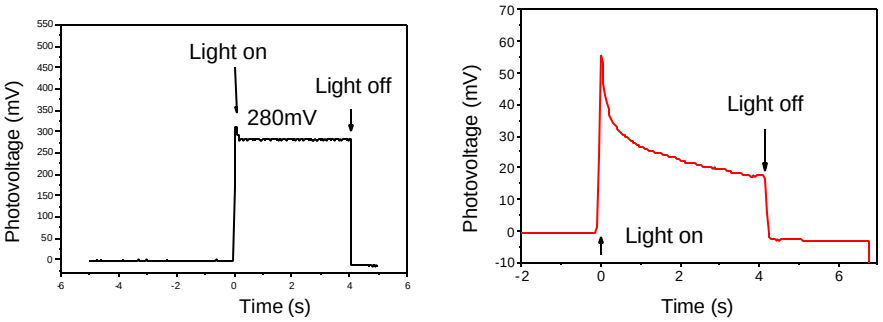

Figure 28. Liquid PPD pre- and post-irradiation responses.

As shown in Figure 28, the post –irradiation response of the liquid LD1 Ru complex N3 PPD (composed of iodine and iodide liquid electrolyte) irradiated to a dose of 100 krad(Si) resulted in ~ 210 mV decrease in photovoltage compared to its pre-irradiation response. This decrease of ~80 % is attributed to severe ionization induced long–term (i.e. permanent) damage. The fall-off of the photovoltage signal with time and during the illumination period of 4 s differed significantly from the post-irradiation photovoltage response of the liquid PPD 1 shown in Figure 27. The post-irradiation response of sample LD1 indicates severe degradation to the generation of photocurrent and the corresponding photovoltage response. However, unlike the substantial persistence of photovoltage beyond the illumination time ($t > 4$ s) exhibited in Figure 27 for sample PPD 1, sample LD1 exhibited minimal broadening in its photovoltage response for $t > 4$ s.

Figure 29 shows the pre-and post irradiated responses of the solid PPD 1A composed of Ruthenium N3 complex. A relative decrease with respect to the control sample of ~20 mV (36%) in output voltage was observed for a gamma-ray dose of 50 krad(Si). In Figure 29, the output voltage responses for the *non-irradiated* solid PPD control (fresh) samples 1A and

2A varied under the same illumination conditions. Control sample 2A showed ~ 2 to 3 mV decrease in its output photovoltage between its initially measured "fresh" results and

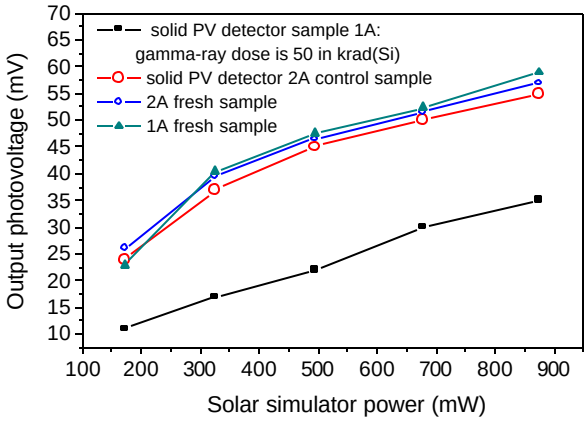

Figure 29. Pre- and post irradiated responses of Ru complex N3 PPDs.

in an identical characterization performed some 10 days after its initial fabrication and characterization. This small decrease in output voltage is most likely due to the aging process in the sample, since the packaging of the PPD films was not designed to rigorously withstand the eventual external migration of trace amounts of moisture and oxygen into the polymer material. These trace amounts of impurities can cause aging-degradation to the polymer properties, which in turn can affect (i.e. decrease) the generation of the photocurrent and photovoltage [56].

Figure 30 represents the responses of the remainder of the N3 PPD sample set irradiated to total doses of 10 and 100 krad(Si). A substantial difference in the PV responses of the N3 PPD devices in Figure 30 is noted when compared to their non-irradiated control (fresh) sample(s) PV baseline values. Following irradiation there is ~ 40 mV decrease in the output photovoltage for PPD 1 and ~ 10 mV decrease in the output of PPD 2 (for illumination powers > 800 mW), again indicating that these PPDs were affected by the gamma-ray irradiations. The consolidated output PV responses for the N3 detectors following irradiation is shown in Table 3. The limited data in Table 3 suggests that for a

dose above 51 krad(Si), the reduction in photovoltage may not scale with increasing dose. At least two interpretations may be construed from this very preliminary and limited data set: 1) that the effect of radiation on the output PV saturates over the range from 51 to 100 krad(Si); and/or, 2) that the radiation induced change in the detector output PV may be nonlinear. The former rather than latter effect is considered to be more likely but in either case, a larger sample set allowing the collection of additional total dose points above and below 100 krad(Si) is required to substantiate these very preliminary trends. Considering that the maximum degradation of the photovoltage of N3 PPD was 36% +/- 5% this extent of degradation in first generation devices would indicate that improvements to increase the radiation resistance of PPDs are quite possible. By chemically altering the polymer composition, it is also possible that the polymer material wavelength response can be extended to result in photodetectors operating at longer

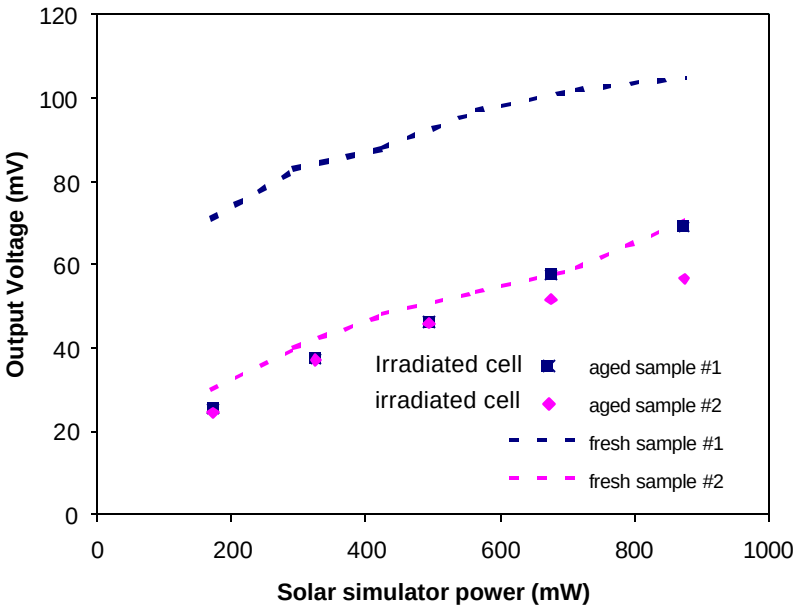

Figure 30. Pre-and post-irradiation characterizations for N3-PPDs 1 and 2.

wavelengths. The realization of photodetectors hardened to ionizing radiation and operating at longer wavelengths will be of benefit to next generation space systems.

Table 3. Ionization induced PV losses in solid N3 PPDs.

PPD	DOSE [RAD(SI)]	PEAK PV DECREASE (%)
2	10	20
1A	51	36
1	100	34

9.3 Pre- and Post Irradiation Reponses of AFRL/MLBP PPDs

Three AFRL/MLBP solid PPDs were irradiated by gamma-rays. The PPDs were composed of self-assembled films consisting of poly (p-phenylene vinylene) (PPV) and sulfonated polystyrene (SPS) as shown in Figure 31.

(a)

Aluminum
(PPV/SPS)$_{30}$
ITO
Glass Substrate

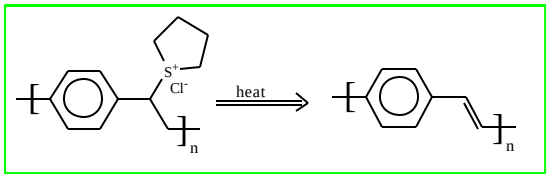

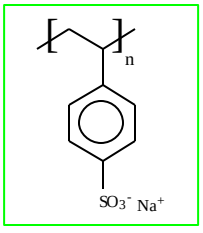

(b) (c)

Figure 31. AFRL/MLBP PPDs. (a) a PPD composed of 30 bilayers of PPV/SPS is shown, (b) and (c) show chemical representations for PPV and SPS, respectively.

The PPD substrates consisted of glass slides (1.0 in. x 1.5 in.) with patterned ITO strips deposited on the surface to serve as transparent electrodes. The polymer layers were deposited by sequentially dipping the substrate into aqueous solutions of the appropriate layer. Aluminum layers were then evaporated perpendicular to ITO strips which served as top electrodes. During their characterization the devices were illuminated through the "back" of the device allowing light to pass through the glass slide and the ITO transparent electrode and eventually absorbed by the polymer layer. The Control PPD was handled and exposed to the same ambient conditions (excluding irradiation by gamma-rays) as experienced by the three irradiated samples. The details for the fabrication and characterization of the devices are reported elsewhere [57,58]. The preliminary analysis of the post-irradiation data indicated that these PPDs exhibited a significant decrease in external quantum efficiency (EQE) over the spectral range of ~275-1150 nm. Figure 32 shows the pre- and post external quantum efficiency (EQE) for PPD 020601 (sample A) irradiated to a dose of 100 krad(Si) . The EQE falls off more rapidly in the irradiated sample and exhibits an order of magnitude decrease in EQE at 500 nm.

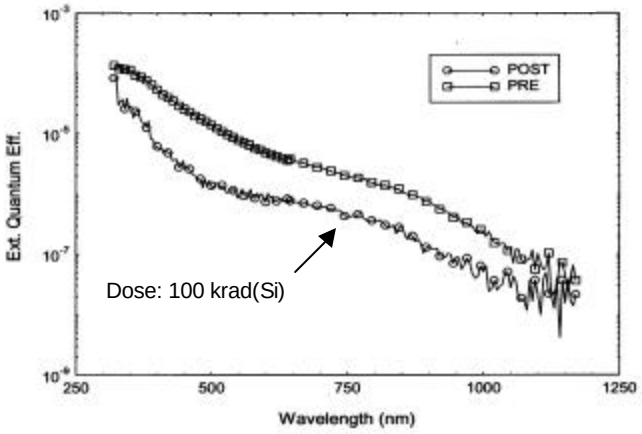

Figure 32. PPV/SPS PPD-sample A pre- and post- irradiation EQE responses.

The changes observed for the EQE of the entire PPV/SPS irradiated sample set is shown in Figure 33. Following irradiation, all sample EQE responses were generally depressed relative to the control sample. A lower ratio for the irradiated samples is indicative of greater reduction in the EQE resulting from the ionization process. An interesting feature was observed in the PPD sample 060201-A [irradiated to 100 krad(Si)] response for wavelengths extending from approximately the visible to the near infrared region (i.e. ~630 nm < λ < 1000 nm). The behavior in sample 060201-A over this region is contrary to expectations, since the EQE for the sample would be expected to scale with dose generally decreasing for increasing dose. As may be observed in Figure 33, while the EQE did decrease over all wavelengths for Sample A, the EQE response is depressed less over the visible to near IR wavelengths compared to the responses of the other two irradiated samples (C and B)

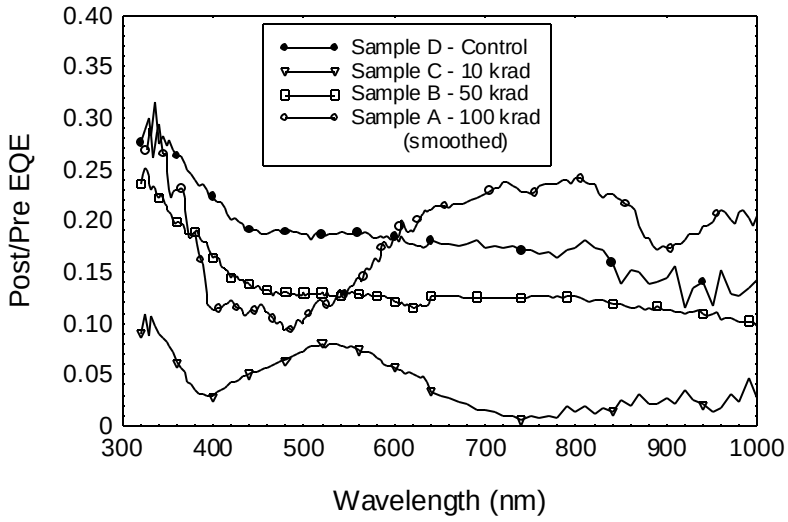

Figure 33. PPV/SPS PPD post- to pre- irradiation EQE ratios.

as well as the control sample (D). The greatest depression in EQE was observed in sample C, irradiated to a dose of 10 krad(Si), while sample B, which received a dose of 50 krad(Si) also had a depressed ratio but was comparable in line-shape to the non-irradiated control sample (D). Additional studies would be required to understand the complex behavior exhibited by the samples. It is sufficient to note that like all Ru Complex PPDs, the PPV/SPS PPDs also degraded in the presence of ionizing radiation.

Figure 34 shows the effects of gamma-ray irradiation on the short-circuit current (Isc) for

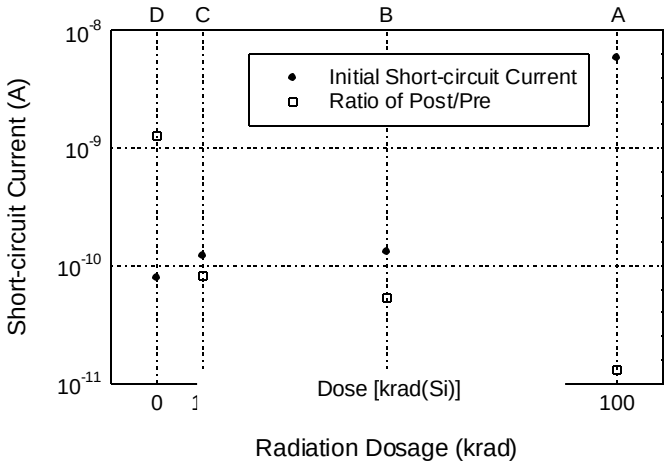

the three irradiated PPV/SPS PPDs. Prior to irradiation the short-circuit current varied significantly in the control sample (D) and in the three pre-irradiated samples, perhaps again indicating the onset of aging effects or perhaps fabrication inconsistencies

Figure 34. PPV/SPS PPD initial and post- to pre-irradiation short-circuit current ratios.

between the individual samples. As may be observed, all Isc values were lower in the post-irradiation measurements, presumably due to the exposure of the PPDs to ambient light and atomic oxygen. However, the Post/Pre (Post-irradiation/Pre-irradiation) ratios in the irradiated samples were two to 10 times smaller for the irradiated samples compared to the non-irradiated control sample. This conclusively indicates that the PPDs experienced gamma-ray induced degradation. As may be observed, the Post/Pre ratio appeared to scale (i.e. ratio decreased) with increasing dose indicating that Isc was affected by the presence of ionizing radiation.

Figure 35 is a similar representation for the pre- and post- irradiation open-circuit voltage (Voc) for the four PPDs (sample D served as the control sample). The trend in the Post/Pre ratio is not as pronounced as was observed in the short-circuit current ratios shown in Figure 34. The initial (pre-irradiation) voltage values are highly scattered which was reportedly not unusual for these devices. However, the most significant change in the ratio is again for the PPDs exposed to doses of 10 and 100 krad(Si). The control PPD and the PPD sample irradiated to 50 krad(Si) exhibited comparable values for both the initial Voc value and in the ratio of post- to pre- Isc.

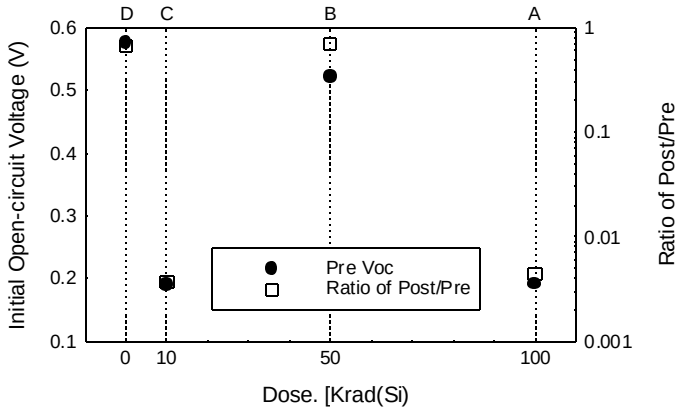

Figure 35. PPV/SPS PPD post- to pre-irradiation open circuit voltages.

10.0 CONCLUSIONS

All ruthenium complex N3 and PPV/SPS polymer photo-detectors exhibited reductions in their output photovoltages and decreases to their photocurrents following irradiation by gamma-rays [59]. The decreases in photovoltages for all devices were long-lived or permanent, with no observed recovery in the time frame of the studies. The pre-and post-irradiation response–behavior varied in identical sample sets and is believed in part due to independent deterioration of the polymer materials via aging-exposure to the ambient atmosphere (e.g. atomic oxygen) and moisture. Aging can affect the stability of PPD photochemistry and photo physical stability of hole transport materials thus reducing the detector charge transport properties. The deterioration was mainly attributed to less than ideal packaging of some of the samples, allowing interaction of some samples with the ambient environment.

Since the photodetector sample size available for the irradiation study was very limited, a clear and statistically based interpretation of the ionization–induced effects in both the

ruthenium complex and PPV/SPS devices proved difficult, especially in determining the scaling response of the PPD output photovoltages with applied dose. Certain of the Ru complex PPD data suggests that a combination of aging and long term if not permanent damage caused by the ionization processes was responsible for limiting the ability of the N2 and N3 dye molecules to fully regenerate under illumination. Degradation was especially pronounced in liquid PPDs where the data suggested that prolonged relaxation times following pulse photo illumination may have resulted from charge trapping and a reduction in the effective conductivity of the charge transport material.

Three AFRL/MLBP poly(p-phenylene vinylene)-sulfonated polystyrene photodetectors were irradiated at incremental doses of 10, 51 and 100 krad(Si). All samples exhibited a EQE decrease over the wavelength range of ~275-1150 nm. However, the EQE was observed to fall off more rapidly in the 100 krad(Si) irradiated sample which exhibited an order of magnitude decrease in EQE at ~500 nm. Interestingly, this particular sample was less depressed in its EQE over the visible -near IR wavelengths (630 nm $< \lambda <$ 1000 nm). The data observed for the elevated dose suggest a potential for realizing radiation resistant devices at longer wavelengths. The data also indicates that trap filling may have also occurred at the onset of irradiation (i.e. at lower doses). The appearance of a small relative resistance to ionizing radiation in the visible to near IR wavelengths could be also be due in part to the formation of new mid-gap states caused by the irradiation. These data can be construed as another positive indication that the focused development of improved radiation resistant–long wavelength PPDs may soon prove feasible

The short-circuit current in the PPV/SPS samples was also observed to decrease with increasing dose, while post-irradiation/pre-irradiation ratios indicated significant damage introduced by the gamma-rays for open circuit voltages measured for devices irradiated at doses of 10 and 100 krad(Si). This data again appears to coincide with the reduction in device conductivity and decrease in EQE.

Of significant interest is that the radiation induced reduction in the output photovoltage for the NanoSonic fabricated Ru complex N3 devices appeared to saturate between 51-100 krad(Si)

which is an indication that this material may also be potentially resistant to ionizing radiation at higher doses and perhaps at longer wavelengths. By chemical modification of polymer materials, the absorption maximum may be shifted to shorter or longer wavelengths, thus determining the detector spectral wavelength response. However, additional studies are required incorporating larger sample sizes of improved next-generation PPDs, allowing additional data collection above and below 100 krad(Si) total dose in order to better understand and ascertain the exact physics involved.

Considering that the polymer photodetectors investigated were primarily based on variations or improvements made to newly emerging or novel PV solar cell materials and designs, the expectation for realizing focused near-term development of radiation resistant polymer–based photodetectors at longer wavelengths is excellent. The data and results of the investigation strongly indicated that the use of molecular self- assembly processes can be used to improve the PPD quantum efficiencies and for extending the spectral response via chemical alteration of the polymer material. Development of a reliable, radiation resistant polymer based detector operating over near to mid- IR wavelengths will undoubtedly find widespread use in space system applications.

11.0 RECOMMENDATIONS

Based on the results of the investigation, the following recommendations are made:

Emphasis and priority should be placed on developing photo-stable PPDs operating at near- to mid- IR wavelengths with improved quantum efficiencies and response times. Also of importance is the development of hermetic packaging techniques suitable for insertion of PPDs in space applications.

In order to better understand the interaction of ionizing radiation with polymer PPDs, additional gamma-ray irradiation studies conducted at higher doses with larger material and device samples sizes should be enjoined to assimilate and increase the data base for accurate modeling of the responses and determination of the extent of radiation-induced degradation processes.

Since electrons and protons are the majority of particles encountered by satellites in the near-Earth space radiation environment, the study of the radiation-induced effects by one or both of these particles in conjunction with additional gamma-ray total dose irradiations should be pursued. The data would greatly assist in bounding and understanding the degradation processes expected of PPDs operating in the natural space environment.

The diversity of emerging polymeric materials suitable for fabricating PPDs is steadily increasing. The extremely limited data base existing for radiation-induced effects in state-of-the-art polymer materials and devices should be expanded and enriched by investigating the radiation resistance of a variety of emerging PPD devices based on different polymer material moieties.

Clearly, the time for economically impacting the rapid development of radiation resistant-long wavelength photodetectors, is in the early stages of emerging polymer –photonics technology development. The research momentum realized in this initial investigative effort should be expediently continued.

REFERENCES

1. U. Bach, D. Lupo, J. E. Moser, F. Weissortel, J. Salbeck, H. Spreizer and M. Gratzel, "Solid-State Dye- Sensitized Mesoporous TiO_2 Solar Cells with High Photon-to-Electron Conversion Efficiencies", *Nature*, Vol. 395, 583-5, (1998).

2. T. Zeng, R. Claus, Y. Liu, F. Zhang, W. Du and K. L. Cooper, "Piezoelectric Ultrathin Polymer Films Synthesized by Electrostatic Self-Assembly Processing", *Smart Mater. Struct.*, Vol. 9, No.6, 801-4, (2000).

3. K. Kalyanasundaram and M. Gratzel, "Application of Functionalized Transition Metal Complexes in Photonic and Optoelectronic Devices", *Coordination Reviews* Vol. 177, 347-414, (1998).

4. A. Mazer, Solar Cells, An Introduction to Crystalline Photovoltaic Technology, Kluwer, New York (1997).

5. T. Zeng, Studies on Preparation and Characterization of Titania Nanocrystallite and its Morphological Effect on Photocatalytic Oxidation of Phenol, Tsinghua University, Beijing, Ph.D. Dissertation (1998).

6. Y. Liu, A. Wang and R. O. Claus, "Molecular Self-Assembly of TiO_2-Polymer Nanocomposite Films", *J. Physical Chemistry B* Vol. 101, 1385-8, (1997).

7. Y. Liu and R. O. Claus, 'Nanoparticle-Polymer Thin-Film Self-Assembly", Wright Laboratory Workshop WPAFB, OH, (March 1998).

8. Y. Liu, A. Wang, R. Claus and E. Jiang, "Molecular Self-Assembly of Fe_3O_4/Polyimide Nanocomposite Films", Magnetic Ultrathin Films, Multilayers and Surfaces - 1997 MRS Symposium 39-47, Boston, (December 1997).

9. R. Claus and Y. Liu, "ESA Fabrication Methods for Materials and Devices", Seminar at Institute for Defense Analyses (November 1997).

10. T. Zeng, W. Du, F. Zhang, A. Rosidian, R. O. Claus, Y. Liu and K. L. Cooper, "Fabrication of Piezoelectric Ultrathin Films for MEMs and Sensors by the Electrostatic Self-Assembly Process", 12th International Workshop on Structural Health Monitoring, Stanford University, (September 1999).

11. Y. Liu, Y-X. Wang and R. O. Claus, "Layer-by-Layer Ionic Self-Assembly of Au Colloids into Multilayer Thin Films with Bulk Metal Conductivity", *Chem. Phys. Lett.*, Vol. 298, 315-9, (1998).

12. A. L. Linsebigler, G. Lu and J. T. Yates, "Photocatalysis on TiO_2 Surfaces: Principles, Mechanisms and Selected Results", *Chem. Rev*., Vol. 31,735-58, (1995).

13. Y. Liu and R. O. Claus, "Strong Enhancement of Optical Absorbance From Ionic Self-Assembled Multilayer Thin Films of Nanocluster Pt and Polymer Dye", *Journal of Applied Physics*, Vol. 85, No.1, 419-24, (1999).

14.C. R. Rice, M. D. Ward, M. K. Nazeeruddin and M. Grätzel, *N. J. Chem.*, Vol. 24: 651-652.(2000).

15. L. M. Peter, K. G. U. Wijayantha, *Electrochimica Acta* Vol.45, 4543-51, (2000).

16. David Cahen and Cary Hodes, *J. Phys. Chem. B*, Vol.104, 2053-59, (2000).

17. R. Huber, S. Sporlein, J. E. Moser, and M. Grätzel, *J. Phys. Chem. B*, Vol. 104: 8995-9003, (2000).

18. J. Nelson, *Physical Review B*, Vol. 59, No.23,: 15374-80, (1999).

19. E. W. Taylor, "Space Effects on Fiber Optics Systems," NASA SP-473, The Long Duration Exposure Facility, Mission 1 Experiments, edited by L. G. Clark et al., Washington, DC, (1984).

20. D. S. McKnight, R. E. Dueber, E. W. Taylor, "Space Debris and Micrometeorite Events Experienced by WL Exp #701 In Prolonged Low-Earth Orbit," *J. Geophysical Research - Space Physics*, Vol. 96, No. A6, (June 1991).

21. E. W. Taylor, J. N. Berry, A. D. Sanchez, R. J. Padden, S. A. DeWalt, S. P. Chapman, "First Operational Space Fiber Optic Links Orbited Aboard the Long Duration Exposure Facility - Lessons Learned," *Proc. AFCEA DoD Fiber Optics '92*, (Mar 1992).

22. E. W. Taylor, "Performance of the First Operable Fiber Optic Systems in Prolonged Space Orbit", *SPIE,* Vol. 1691, (April 1992).

23. E. W. Taylor, J. N. Berry, R. J. Padden, A. D. Sanchez, and S. P. Chapman, "Preliminary Analysis of WL Exp #701, Space Environment Effects on Operating Fiber Optic Systems", *NASA CP 3134, LDEF - 69 Months in Space - Part III*, (May 1992).

24. A. R. Johnston and E. W. Taylor, "A Survey of the LDEF Fiber Optic Experiments", *JPL D-10069*, Jet Propulsion Laboratory, California Institute of Technology, (Nov. 1992).

25. E. W. Taylor, J. M. Emmes, C. E. Barnes, and F. Wiczer, "Behavior of Irradiated Plastic Clad Silica Fibers at Low Temperatures", *Proc. Compte-Rendu,* Paris, FR, (October 1980).

26. E. W. Taylor, L. J. Myatt, and J. D. Wiltse, "Low Temperature Gamma Irradiation of Polymer Coated Optical Waveguides", *SPIE,* Vol. 404, (May 1983).

27. E. J. Friebele, E. W. Taylor, G. Turquet de Beauregard, J. Wall, and C. E. Barnes, "Interlaboratory Comparison of Radiation Induced Attenuation in Optical Fibers, Part I. Steady State Exposures**",** IEEE/OSA, *J. of Lightwave Technology,* Vol. 6, No. 2, 165-171, (February 1988).

28. E. W. Taylor, E. J. Friebele, H. Henschel, R. H. West, J. A. Krinsky, C. E. Barnes, "Interlaboratory Comparison of Radiation-Induced Attenuation in Optical Fibers. Part II: Steady State Exposures", *IEEE/OSA J. Lightwave Technol.*, Vol. 8, No. 6, (June 1990).

29. E. W. Taylor, E. J. Friebele, H. Henschel, R. H. West, J. Krinsky, C. E. Barnes "NATO Nuclear Effects Task Group Interlaboratory Comparison of Radiation Induced Attenuation in Optical Fibers. Part II: Steady State Exposures", NATO Technical Report AC/243 (Panel 4) TR/6, RSG. 12 on Fiber and Associated Integrated Optic Technology, (July 1991).

30. E. W. Taylor, R. Claus, K. Cooper, L. R. Taylor, "Gamma-Ray Irradiation and Responses of Electrostatically Assembled Electro Optic Polymer Materials", *SPIE* Vol. 4547, Toulouse, France, (September 17-21, 2001).

31. J. Zetts, J. Grote, J. Huddleston, R. Nelson, F. Hopkins E. Taylor, "Conductive Cladding Materials for Optimized Performance of Nonlinear Optic Polymers", Toulouse, France, (Sept. 17-21, 2001, unpublished).

32. E. W. Taylor. "Inorganic and Polymer Photonic Sensor Technologies in Space Missions", *Proc. 18th IEEE Instrumentation and Measurement Technology Conference*, Vol. 3, ISBN 0-7803-6646-8, Budapest, Hungary, (May 21-23, 2001).

33. E. W. Taylor, *"Radiation Effects"*, Chapter 14.1, in: Properties of Lithium Niobate**,** Edited by K.K. Wong , *IEE EMIS Datareviews Series*, No. 28, 359-71, (2002).

34. E. W. Taylor, A. Pirich, L. R. Taylor, "Qualifying Photonics for Space Environments", *Proc. 47th ISA International Instrumentation Symposium*, Denver Colorado, (May 2001).

35. E. W. Taylor, Editor, *SPIE* *Photonics for Space Environments Conference VII*, *SPIE* Vol. 4134, San Diego, CA, (August 1, 2000).

36. E. W. Taylor, J. Grote, J. Zetts, J.E. Winter , A. D. Sanchez , D. Craig, "In Situ High Energy Proton Irradiation of Nonlinear Organic Modulator Materials for Space Environments", *SPIE* Vol. 4134, San Diego, CA, (August 1, 2000).

37. J. Grote, E. W. Taylor, J. Zetts, J. Winter, A. D. Sanchez, D. Craig, F. Hopkins, "Optical Transmission and Thermal Heating Effects Due to Irradiation of Nonlinear Optic and Conductive Polymers for Spaced Based Electrooptic Applications", *SPIE* Vol. 4134, San Diego, CA, (August 1, 2000).

38. E. W. Taylor, "An Overview of Research and Development of Polymer Materials for Space Applications", *Proc. 46th ISA International Instrumentation Symposium*, (April 2000).

39. E. W. Taylor, "Radiation Effects Observed in Selected Guided Wave Devices", in SPIE CR-45 Integrated Optics and Optoelectronics-Critical Reviews of Optical Science and Technology, K. K. Wong and M. Razaghi, eds., ISBN 08194-1005-5, (January 21-23, 1993).

40. E. W. Taylor, "Radiation Induced Effects in Guided Wave Devices", *SPIE*, Vol. 1794, 54-61, (September 1992).

41. E. W. Taylor, "On the Measurement of Radiation Induced Crosstalk in Polarization Preserving Optical Fibers and Directional Coupler Waveguides", *Proc. European*

Space Agency / IEEE Radiation Effects on Components and Devices, Vol. 15, (September 1991).

42. E. W. Taylor, R. J. Padden, A. D. Sanchez, S. P. Chapman, J. N. Berry, S. A. DeWalt, "Radiation Induced Crosstalk in Guided Wave Optical Devices", *SPIE*, Vol. 1474, (April 1-3, 1991).

43. E. W. Taylor, "Behavior of Coupled Waveguide Devices in Adverse Environments", *SPIE*, Vol. 1314, (April 1990).

44. E. W. Taylor , "Ionization-Induced Refractive Index and Polarization Effects in $LiNbO_3$:Ti Directional Coupler Waveguides", *IEEE/OSA J. Lightwave Technol.*, Vol. 9, No. 3,(March 1991).

45. E. W. Taylor, "Geminate Recombination Behavior of a X-Ray Irradiated Single Mode $LiNbO_3$:Ti Waveguide Operating at 1300 nm", *J. Opt. Comm.*, Vol. 9, (1988).

46. K. L. Cooper, R. O. Claus, " Self-Assembled Radiation Resistant Thin Films and Devices", DASG60-00-M-0096, (October, 2000).

47. S. R. Forrest, "Active Optoelectronics Using Thin Film Organic Semiconductors", *IEEE J. Selected Topics in Quantum Electronics*, Vol. 6, No.6, (Nov/Dec 2000).

48.G. Barbarella, L. Favaretto, G. Sotgiu, M. Zambianchi, C. Arbizzani, A. Bongini, M. Mastragostino, G. Gili, R. Cingolani, " Chemically and Thermally Stable Photo and Electroluminescent Thiopene-Based Materials", in: Photonics for Space Environments VII, E. W. Taylor, Ed., *SPIE* Vol. 4134, (August 2000).

49. M. A. Baldo, D. F. O'Brien, M. E. Thompson, S. R. Forrest, "Highly Efficient Phosphorescent Emission from Electroluminescent Devices", *Nature*, Vol. 395, (1998).

50. F. Papadimitrakopoulous, X.-M. Zhang, K. A. Higginson, “Chemical and Morphological Stability of Aluminum Tris (8- Hydroxyquinoline)(AlQ3): Effects in Light Emitting Diodes”, *IEEE J. Selected Topics in Quantum Electronics*, Vol. 4, No.1, (Jan/Feb 1998).

51. G. Gu, S. R. Forrest, “Design of Flat Panels Based on Organic Light-Emitting Diodes”, *IEEE J. Selected Topics in Quantum Electronics*, Vol. 4, No.1, (Jan/Feb 1998).

52. A. J. Pal, T. P. Ostergard, R. M. Osterbacka, J. Paloheimo, H. Stubb, “ Langmuir-Blodgett Films of Conjugated Polymers: Electroluminescence and Charge Transport Mechanisms”, *IEEE J. Selected Topics in Quantum Electronics*, Vol. 4, No.1, (Jan/Feb 1998).

53. P. W. Blom, M. J. M. de Jong, “ Electrical Characterization of Polymer Light Emitting Diodes”, *IEEE J. Selected Topics in Quantum Electronics*, Vol. 4, No.1, (Jan/Feb 1998).

54. S. K. Dey, N. B. Manik, S. Bhattacharya, A. N. Basu, *Synthetic Metals*, Vol. 118, 19-23, (2000).

55. E. Pinotti, A. Sassella, A. Borghesi, T. Turbino, “Electrical Characterization of Organic Semiconductors by Transient Current Methods”, *Synthetic Metals*, Vol. 122, 169-71, (2001).

56. J. Steiger, S. Krag, R. Schmechel, H. von Seggern, “Aging Induced Traps in Organic Semiconductors”, *Synthetic Metals*, Vol. 122, 49-52, (2001).

57. M. F. Durstock, B. Taylor, R. J. Spry, L. Chiang, S. Reulbach, K. Heitfeld, J. W. Baur, " Electrostatic Self-Assembly as a Means to Create Organic Photovoltaic Devices", *Synthetic Metals*, Vol. 116, 373-77, (2001).

58. J. W. Baur, M. F. Durstock, B. E. Taylor, R. J. Spry, S. Reulbach, L. Y. Chiang, "Photovoltaic Interface Modification via Electrostatic Self-Assembly", *Synthetic Metals*, Vol. 121, 147-48, (2001).

59. E. W. Taylor, D. Le, M. F. Durstock, B. E. Taylor, R. O. Claus, T. Zeng, C. P. Morath, D. Cardimona, "Space Radiation Induced Effects in Polymer Photodetectors", *SPIE*, Vol. 4128, (July 2002).

APPENDIX A XPD Data

Table A-1. Concentration of element components on the surface of TiO_2 - dye photovoltaic film.

Atomic Concentration Table

File: ty2 titanuim dioxide and rutheenium complex 2 Sintered
Lens: Small Area Omni-Focus Source: Standard

Element	Area (cts-eV/s)	Sensitivity Factor	Concentration (%)
C1s	5563	0.296	27.37
O1s	23261	0.711	47.65
Ru3d	912	4.273	0.31
N1s	1313	0.477	4.01
Cl2p	1745	0.891	2.85
Ti2p	24472	2.001	17.81

Table A-2. Atomic concentration of elements for the TiO_2 - dye at 5 nm depth.

Atomic Concentration Table

ty12 titanuim dioxide and rutheenium complex 2 Sintered
Small Area Omni-Focus Source: Standard

Element	Area (cts-eV/s)	Sensitivity Factor	Concentration (%)
C1s	3311	0.296	19.13
O1s	21801	0.711	52.44
Ru3d	477	4.273	0.19
N1s	896	0.477	3.21
Cl2p	972	0.891	1.87
Ti2p	27096	2.001	23.16

Table A-3. Atomic concentration of elements for the TiO_2 - Dye at 10 nm depth.

Atomic Concentration Table

File: ty14 titanuim dioxide and rutheenium complex 2 Sintered
Lens: Small Area Omni-Focus Source: Standard

Element	Area (cts-eV/s)	Sensitivity Factor	Concentration (%)
C1s	3099	0.296	16.13
O1s	25355	0.711	54.95
Ru3d	508	4.273	0.18
N1s	773	0.477	2.50
Cl2p	777	0.891	1.34
Ti2p	32320	2.001	24.89

Table A-4. Atomic concentration of elements for the TiO_2 -dye at 40 nm depth.

Print AC Table | Print AC Table | Exclude Region | Atomic Concentration | Display Curve | More Softkeys | AC to AC Summary | Exit

a User Settings Previous New
c Mode Area Height d Baseline Linear Integrated
e Regions C1 O1 Ru1 N1 Cl1 Ti1

b Element Name

File: ty31
Lens: Small Area Omni-Focus

Atomic Concentration Table
sintered titanium dioxide and rutheenium complex 2
Source: Standard

Element	Area (cts-eV/s)	Sensitivity Factor	Concentration (%)
C1s	1425	0.296	7.91
O1s	26193	0.711	60.51
Ru3d	506	4.273	0.19
N1s	374	0.477	1.29
Cl2p	369	0.891	0.68
Ti2p	35846	2.001	29.42

BIBLIOGRAPHY

Bach, U., Kruger, J., Gratzel, M., "The Concept of Dye-Sensitized Mesoporous Solid-State Heterojunction Solar Cells", *SPIE*, Vol. 4108, 1-7, (2001).

Borsenberger, P. M., Gruenbaum, W. T., Magin, E. H., Visser, S. A., Schildkraut, D. E., "Hole Trapping in Molecularly Doped Polymers", *J. Poly. Sci. B*, Vol. 37, 349-356, (1999).

Briskman, B. A., "Radiation Effects in Thermal Properties of Polymers, An Analytical Review, I. Polyethylene", *Nuclear Instruments and Methods in Physics Research B*, Vol. 185, 116-22, (2001).

Burnside, S., Winkle, S. Brooks, K, Shklover, V. Gratzel, M., Hinsch, A, Kinderman, R, Bradbury, C., Hagfeldt, A., Petterson, H., "Deposition and Characterization of Screen-Printed Porous Multi-Layer Thick Film Structures from Semiconducting and Conducting Nanomaterials for Use in Photovoltaic Devices", *J. Mater. Sci. Mater. Electron.*, Vol. 11, No. 4, 355-62, (June 2000).

Brandrup, J., Immergut, E. H., Polymer Handbook, 2nd ed., John Wiley & Sons, (1975).

Czeremuszkin, G., Latreche, M., Wertheimer, M. R., "Charging/Discharge Events in Coated Spacecraft Polymers During Electron Beam Irradiation in a Scanning Electron Microscope", *Nuclear Instruments and Methods in Physics Research B*, Vol. 185, 88-99, (2001).

Das, G. P., Vaia, R., Yeates, A. T., Dudis, D. S., "A Theoretical Model for Excited State Absorption", *Synthetic Metals*, Vol. 116, 281-3, (2001).

Gratzel, M., "Sol-Gel Processes TiO_2 Films for Photovoltaic Applications", *J. Sol Gel Technol.*, Vol. 22, No. 1-2, (September 7-13, 2001).

Gratzel, M.,"Photoelectrochemical Cells", *Nature*, Vol. 414, No. 6861, 338-44, (2001)

Gratzel, M., "Perspectives for Dye- Sensitized Nanocrystalline Solar Cells", *Prog. Photovolt. Res. Appl*, , Vol. 8, No. 1, 171-85, (Jan.-Feb. 200).

Jones, M. Jr., Organic Chemistry, W. W. Norton & Co., N. Y., (1997).

Kruger, J., Plass, R., Le Cevey, P., Piccirelli, M., Gratzel, M., Bach, U., "High Efficiency Solid-State Photovoltaic Device Due to Inhibition of Interface Charge Recombination", *Appl. Phys. Lett*., Vol. 79, No.13, 2085-7, (September 24, 2001).

Liu, Y., Wang, A., Claus, R., "Molecular Self-Assembly of TiO_2/Polymer Nanocomposite Films", *J. Phys. Chem. B*, Vol. 101, No. 8, 1385-88, (February 20, 1997).

Mandowski, A., "Charge Carrier Trapping in a One-Dimensional System", *IEEE Trans. on Dielectrics and Electrical Insulation*, Vol. 8, No. 6, 1007-10, (December 2001).

Mark, J. E., Polymer Data Handbook, Oxford University Press, N. Y., (1999).

O'Regan, B, Schwartz, D. T., Zakeeruddin, S. M., Gratzel, M., "Electrodeposited Nanocomposite n-p Heterojunctions for Solid-State Dye-Sensitized Photovoltaics", *Adv. Mater.*, Vol.12, No.17, 1263-7, (September 1, 2000).

Salamone, J. C., Concise Polymeric Materials Encyclopedia, CRC Press, (1999).

Sinke, W. C., Wienke, M. M., "Solid-State Organic Solar Cells", *Nature*, Vol. 395, 544-5, (October 8, 1998).

Skotheim, T. A, Handbook of Conducting Polymers, Vols. I & II, Marcel Dekker, Inc., N. Y. (1986).

Zaharescu, T., "Thermodynamic Assessment of γ-Irradiated NBR/Synthetic Elastomer Blends", *Nuclear Instruments and Methods in Physics Research B*, Vol. 185, 136-9, (2001).

DISTRIBUTION LIST

DTIC/OCP
8725 John J. Kingman Rd, Suite 0944
Ft Belvoir, VA 22060-6218 1 cy

AFRL/VSIL
Kirtland AFB, NM 87117-5776 1 cy

AFRL/VSIH
Kirtland AFB, NM 87117-5776 1 cy

International Photonics Consultants, Inc
30 Tierra Monte NE
Albuquerque, NM 87122 1 cy

Official Record Copy
AFRL/VSSS/Lt Dang Le 1 cy